

Intersectin-1 interacts with the golgin GCC88 to couple the actin network and Golgi architecture

Christian Makhoul[†], Prajakta Gosavi[†], Regina Duffield, Bronwen Delbridge, Nicholas A. Williamson, and Paul A. Gleeson*

Department of Biochemistry and Molecular Biology and Bio21 Molecular Science and Biotechnology Institute, The University of Melbourne, Melbourne, Victoria 3010, Australia

ABSTRACT The maintenance of the Golgi ribbon relies on a dynamic balance between the actin and microtubule networks; however, the pathways controlling actin networks remain poorly defined. Previously, we showed that the *trans*-Golgi network (TGN) membrane tether/golgin, GCC88, modulates the Golgi ribbon architecture. Here, we show that dispersal of the Golgi ribbon by GCC88 is dependent on actin and the involvement of nonmuscle myosin IIA. We have identified the long isoform of intersectin-1 (ITSN-1), a guanine nucleotide exchange factor for Cdc42, as a novel Golgi component and an interaction partner of GCC88 responsible for mediating the actin-dependent dispersal of the Golgi ribbon. We show that perturbation of Golgi morphology by changes in membrane flux, mediated by silencing the retromer subunit Vps26, or in a model of neurodegeneration, induced by Tau overexpression, are also dependent on the ITSN-1-GCC88 interaction. Overall, our study reveals a role for a TGN golgin and ITSN-1 in linking to the actin cytoskeleton and regulating the balance between a compact Golgi ribbon and a dispersed Golgi, a pathway with relevance to pathological conditions.

Monitoring Editor

Benjamin S. Glick
University of Chicago

Received: May 23, 2018

Revised: Nov 19, 2018

Accepted: Dec 4, 2018

INTRODUCTION

The Golgi complex plays a critical role in the regulation of anterograde, retrograde, and recycling trafficking as well as the posttranslational modification of proteins and lipids. In addition, there is emerging evidence for a role of the Golgi complex in a range of

other cellular processes, including autophagy, cell migration, signaling, metabolism, and DNA repair (Farhan and Rabouille, 2011; Mayingier, 2011; Wilson et al., 2011; Millarte and Farhan, 2012; Luini and Parashuraman, 2016; Gosavi and Gleeson, 2017). Collectively, these functions are mediated by peripheral and integral membrane proteins, as well as lipids, that also regulate Golgi architecture (Gosavi and Gleeson, 2017). The individual stacks of the Golgi apparatus consist of four to eight flattened cisternal membrane structures (Short et al., 2005) with a defined organization of *cis*-, *medial*-, and *trans*-cisternae, where the first represents the cargo entry point from the ER. A characteristic feature of the Golgi complex in vertebrate cells is a ribbon structure, where multiple Golgi stacks are linked laterally to form a twisted, reticular structure that is maintained close to the centrosome by interactions with microtubules (Rios and Borens, 2003; De Matteis et al., 2008). In contrast to the vertebrates, the Golgi ribbon structure is absent in protists and plant and invertebrate cells; rather, in these cells, the Golgi complex is found as individual stacks scattered throughout the cytoplasm. An intact Golgi stack is required for efficient membrane transport (Glick and Nakano, 2009; Brandizzi and Barlowe, 2013), whereas the arrangement of the Golgi in a ribbon architecture does not appear to be necessary for membrane transport; rather it is likely to contribute to a range of other functions (Wei and Seemann, 2010).

This article was published online ahead of print in MBoC in Press (<http://www.molbiolcell.org/cgi/doi/10.1091/mbc.E18-05-0313>) on December 12, 2018.

[†]These authors contributed equally to this work.

Author contributions: P.G., C.M., and P.A.G. conceived the project, designed the experiments, interpreted the data, and wrote the manuscript; P.G. and C.M. performed the majority of the experiments and analyzed the data; B.D. generated recombinant lentivirus and performed the primary neuron experiments; R.D. generated and analyzed the BioID constructs; N.A.W. performed the MS analysis on trypsin digests.

The authors declare no competing financial interests.

*Address correspondence to: Paul Gleeson (pgleeson@unimelb.edu.au).

Abbreviations used: BioID, proximity-dependent biotin identification; BirA*, BirA-R118G; GA, glutaraldehyde; GCC, Golgi coiled-coil protein; GEF, guanine nucleotide exchange factor; ITSN-1, intersectin 1; ITSN-1-S, short isoform of ITSN-1; ITSN-1-L, long isoform of ITSN-1; Lat A, latrunculin A; PFA, paraformaldehyde; Rheb, Ras homologue enriched in brain; TGN, *trans*-Golgi network; UtrCH, Utraphin calponin homology domain; WT, wild type.

© 2019 Makhoul, Gosavi, et al. This article is distributed by The American Society for Cell Biology under license from the author(s). Two months after publication it is available to the public under an Attribution-NonCommercial-Share Alike 3.0 Unported Creative Commons License (<http://creativecommons.org/licenses/by-nc-sa/3.0>).

"ASCB®," "The American Society for Cell Biology®," and "Molecular Biology of the Cell®" are registered trademarks of The American Society for Cell Biology.

The organization of the Golgi ribbon is highly dynamic, and it can be disassembled and reorganized under a variety of conditions, such as mitosis (Nelson, 2000; Colanzi *et al.*, 2003), the repositioning of the Golgi complex to facilitate polarized trafficking and directed secretion, and cilia biogenesis, and is also exploited in pathogen invasion (Kupfer *et al.*, 1983; Yadav *et al.*, 2009). Moreover, loss of the organization of the typical compact Golgi ribbon structure has been associated with a variety of pathological conditions, including neurodegenerative diseases (Gonatas *et al.*, 2006; Rabouille and Haase, 2015; Sundaramoorthy *et al.*, 2015) and cancer (Farber-Katz *et al.*, 2014; McKinnon and Mellor, 2017), highlighting the importance of the ribbon morphology in cellular homeostasis. The architecture of the Golgi ribbon results from interactions of components of Golgi membranes with the microtubule and actin cytoskeletons. While the role of microtubule cytoskeletons in the organization and position of the Golgi ribbon in vertebrate cells is well known (Sutterlin and Colanzi, 2010; Sanders and Kaverina, 2015), the contribution of the actin-based cytoskeletal system to Golgi architecture has only been recognized more recently (Egea *et al.*, 2013). A number of Golgi-localized molecular scaffolds have been identified that interact with the actin cytoskeleton and affect Golgi morphology (see review, Gosavi and Gleeson, 2017). The major classes of Golgi proteins that interact with the actin cytoskeleton are the coiled-coil domain golgins (Goud and Gleeson, 2010; Munro, 2011), including giantin, GM130, golgin-245, and optineurin, the stacking proteins GRASP55/65 (Ramirez and Lowe, 2009), the membrane tether Golgi phosphoprotein 3 (GOLPH3) (Buschman *et al.*, 2015), and the formin FHDC1 (Copeland *et al.*, 2016). Myosins have also been localized to the Golgi complex, which can generate actin-associated tensile forces to modulate the architecture of Golgi membranes and to generate Golgi-derived transport vesicles (Brownhill *et al.*, 2009; Dippold *et al.*, 2009; Miserey-Lenkei *et al.*, 2010; Anitei and Hoflack, 2011). Thus, the ribbon morphology of the Golgi can be regulated by scaffold molecules that interact with actin.

In addition to regulating Golgi architecture and vesicle biogenesis, there is evidence that actin dynamics can also influence signaling pathways at the Golgi. The Golgi structural protein, GOLPH3, not only influences Golgi morphology by an actin-dependent process but also promotes cell survival after DNA damage (Farber-Katz *et al.*, 2014) and appears to modulate mTOR signaling and cell proliferation (Scott *et al.*, 2009), processes that are interlinked. Another example involves the serine/threonine protein kinase (STK16), which is localized to the Golgi and regulates Golgi disassembly and assembly during the cell cycle by modulating actin dynamics (Liu *et al.*, 2017b).

To fully understand the roles of the Golgi in higher-order functions, it is important to identify the molecular players that link Golgi morphology and function. We previously established a novel approach to altering the balance between the Golgi ribbon and Golgi mini-stacks by modulating the dose of a membrane tether or golgin located at the *trans*-Golgi network (TGN), namely GCC88 (encoded by *GCC1*). We demonstrated that a twofold increase in the level of GCC88 in HeLa cells resulted in loss of the compact Golgi ribbon and dispersal of the organelle as mini-stacks throughout the cytoplasm. Conversely, knockdown of GCC88 resulted in a longer Golgi ribbon than in parental HeLa cells (Gosavi *et al.*, 2018). The change in Golgi architecture did not affect membrane transport (Gosavi *et al.*, 2018). Using this system, we demonstrated that the organization of the Golgi ribbon was important in the regulation of autophagy and mTOR signaling (Gosavi *et al.*, 2018). Loss of the Golgi ribbon resulted in a dramatic reduction in mTOR activity and the

induction of autophagy, presumably due to inability to recruit the Golgi pool of mTOR. Here we demonstrate that the molecular mechanism whereby GCC88 negatively regulates the Golgi ribbon involves the actin cytoskeleton, and furthermore, we have identified intersectin 1 (ITSN-1) as a binding partner of GCC88 that is needed to link TGN membranes to the actin cytoskeleton. ITSN-1 is a scaffold molecule involved in endocytosis and actin regulation and also has been implicated in regulating signaling in physiology and in disease (Hussain *et al.*, 2001; Hunter *et al.*, 2013; Herrero-Garcia and O'Bryan, 2017); however, ITSN-1 has not previously been shown to be involved in Golgi dynamics. Significantly, here we identify the long isoform of ITSN-1, which has Cdc42 GEF activity (Hussain *et al.*, 2001), as the relevant isoform that promotes Golgi fragmentation. Our study includes a role for the small GTPase, Cdc42, and myosin motors in maintaining the balance between a compact Golgi ribbon and dispersed Golgi stacks. The pathway described in this report is important in understanding the molecular basis for the loss of the Golgi ribbon in a variety of physiological and pathological processes.

RESULTS

Perturbation of the Golgi ribbon by GCC88 is actin-dependent

We previously showed that overexpression of either tagged or untagged GCC88 results in fragmentation of the Golgi complex (Gosavi *et al.*, 2018). The HeLa cell clone B6, which stably expresses GFP-tagged GCC88 and has a twofold higher level of GCC88 than parental HeLa cells, does not have a compact Golgi ribbon structure but rather a fragmented Golgi dispersed throughout the cytoplasm (Figure 1A; Gosavi *et al.*, 2018). Previously, we demonstrated that the Golgi fragments of HeLa-B6 cells represented Golgi mini-stacks scattered in the cytoplasm and we quantified the extent of Golgi dispersal by optical and electron microscopy (EM), including tomography, and by flow cytometry (Gosavi *et al.*, 2018). Transient expression of GFP-GCC88 in a range of immortalized cells, including CHO cells and the neuroblastoma line SK-N-SH also resulted in dispersal of Golgi structures that costain with the *cis*- and *trans*-Golgi markers (Figure 1B). Quantitation of the dispersal of the Golgi by measurement of the area of the Golgi structures, stained for the Golgi marker GM130, clearly demonstrates a significantly larger surface area in CHO cells, SK-N-SH, cells and HeLa B6 cells expressing GFP-GCC88 compared with the parental cells (Figure 1C). Expression of GFP-GCC88 in day 7 cultured primary mouse neurons also resulted in dispersal of the Golgi ribbon (Figure 1D). Hence, the functional activity of GCC88 in regulating Golgi morphology is conserved across species and is relevant to both immortalized and primary cells.

Both the microtubule and actin cytoskeletons are involved in maintaining the architecture of the Golgi complex (Lowe, 2011). In view of an emerging central role of the actin cytoskeleton in the dynamics of the Golgi morphology, and as there was no obvious difference in overall microtubule staining of HeLa-B6 cells compared with parental HeLa cells (unpublished data), we investigated whether actin promoted the dispersal of the Golgi ribbon in HeLa-B6 cells. Parental HeLa, HeLa-B6 and SK-N-SH cells were treated with the drug latrunculin A (Lat A), which binds to monomeric actin and prevents F-actin assembly (Spector *et al.*, 1983; Coue *et al.*, 1987), and jasplakinolide, which stabilizes actin microfilaments *in vitro* and enhances actin polymerization *in vivo* (Bubb *et al.*, 2000). Significantly, a 30-min treatment with Lat A resulted in a very compact Golgi in HeLa cells and SK-N-SH cells as well as in HeLa-B6 cells (Figure 2A), with a reduction in the area of GM130 positive structures compared

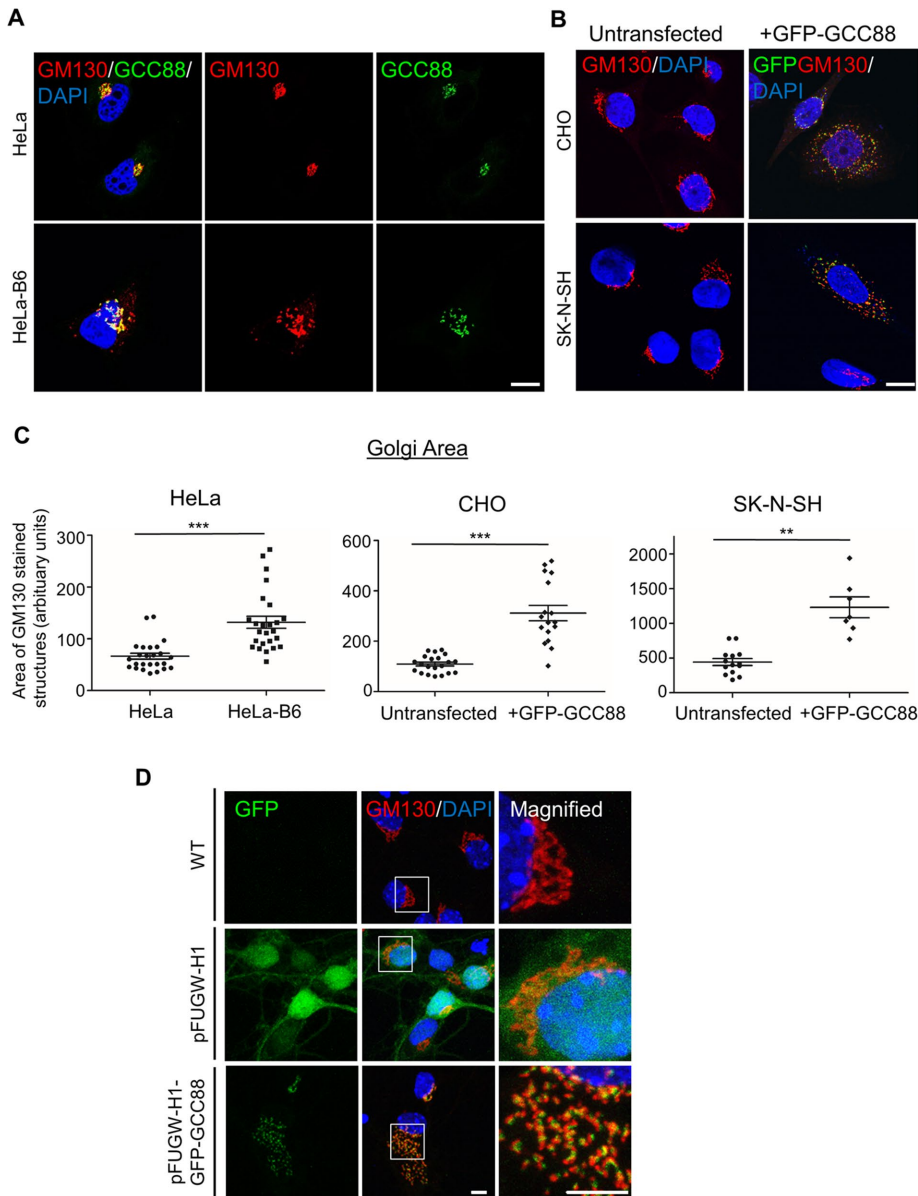


FIGURE 1: GCC88 expression disperses the Golgi ribbon structure into Golgi mini-stacks. (A) Immunostaining of parental HeLa and HeLa-B6 cells with rabbit anti-GCC88 (green; TGN marker) and mouse anti-GM130 (red; cis-Golgi marker) antibodies. (B) CHO or SK-N-SH cells were transfected with GFP-GCC88 for 24 h and monolayers were stained with mouse anti-GM130 antibodies (red). GFP fluorescence was detected in transfected cells. (C) Area of the Golgi defined by the Golgi marker GM130, from A and B. Data from two independent experiments are pooled and expressed as the mean \pm SEM. Each symbol represents an individual cell. Data were analyzed by an unpaired, two-tailed Student's *t* test. ***p* < 0.01, ****p* < 0.001. (D) Primary mouse cortical neurons 7 d in culture were either untransduced (WT) or transduced with pFUGW-H1 or pFUGW-H1-GFP-GCC88 lentivirus for a further 6 d, and monolayers were fixed and stained with GM130 (red). Nuclei were stained with DAPI. Scale bar, 10 μ m, 5 μ m in the enlarged images.

with carrier-treated control cells (Figure 2B), indicating that actin filaments are needed to drive the dispersal of the Golgi ribbon by GCC88. Of note is that LatA treatment also results in some swelling of the cisternae, consistent with previous reports on the effect of LatA (Lazaro-Dieguez *et al.*, 2006), which may be due to the impact of latrunculin on trafficking (Zegers *et al.*, 1998). Treatment of parental HeLa cells with both Lat A and nocodazole simultaneously resulted in dispersed Golgi membranes (Supplemental Figure S1),

demonstrating that the Golgi complex in Lat A-treated cells is dependent on microtubules for its location and compact state. In addition, EM analysis of HeLa-B6 cells demonstrated that the average length of the Golgi cisternae was substantially greater in these cells after treatment with Lat A (Figure 2C), a cisternae length that reflected the Golgi ribbon of parental HeLa cells. Hence the action of Lat A had reversed the phenotype induced by overexpression GCC88.

In contrast, the dispersal of the Golgi in HeLa-B6 cells was maintained in jasplakinolide-treated cells, and jasplakinolide treatment induced extensive dispersal of the compact Golgi in parental HeLa cells and in SK-N-SH cells (Figure 2, A and B). Quantitation revealed a significant increase in the Golgi area following jasplakinolide treatment compared with that in carrier-treated control cells (Figure 2B). Hence actin microfilaments, in the presence of an intact microtubule (MT) array, can mediate disruption of the Golgi ribbon and dispersal of Golgi membranes throughout the cytoplasm. Together, these findings indicate that actin dynamics can dramatically alter the architecture and location of the Golgi membranes in the cytoplasm.

Identification of ITSN-1 as a binding partner of GCC88

To identify the mechanism by which GCC88 influences the Golgi architecture, the *in vivo* proximity-dependent labeling method BioID was employed to identify candidate interactors that could be facilitating this process. We generated a Myc-BirA*-GCC88 fusion protein that was localized at the Golgi in transfected HeLa cells (Figure 3A) and was detected as a 120-kDa species by immunoblotting (Supplemental Figure S2). Addition of biotin to Myc-BirA*-GCC88-transfected cells resulted in the biotinylation of proteins, as detected by streptavidin-488; moreover, the biotinylated proteins localized extensively with the TGN marker p230/golgin-245 (Figure 3A). These immunofluorescence data indicate that the majority of proteins biotinylated by Myc-BirA*-GCC88 are restricted to the Golgi environment. Biotinylated proteins were purified from lysed cells by affinity chromatography using streptavidin and analyzed by mass spectrometry (MS) as described in *Materials and Methods*. As a control in the analyses we included cells transfected with Myc-BirA* (Supplemental Figure S2) alone, and in contrast to the Golgi-localized Myc-BirA*-GCC88, Myc-BirA* protein is distributed throughout the cytosol (unpublished data). In total 32 proteins were identified as unique proteins in Myc-BirA* tagged GCC88 transfected cells but not BirA-alone transfected cells in at least two independent experiments (Supplemental Materials Appendix I), using criteria described

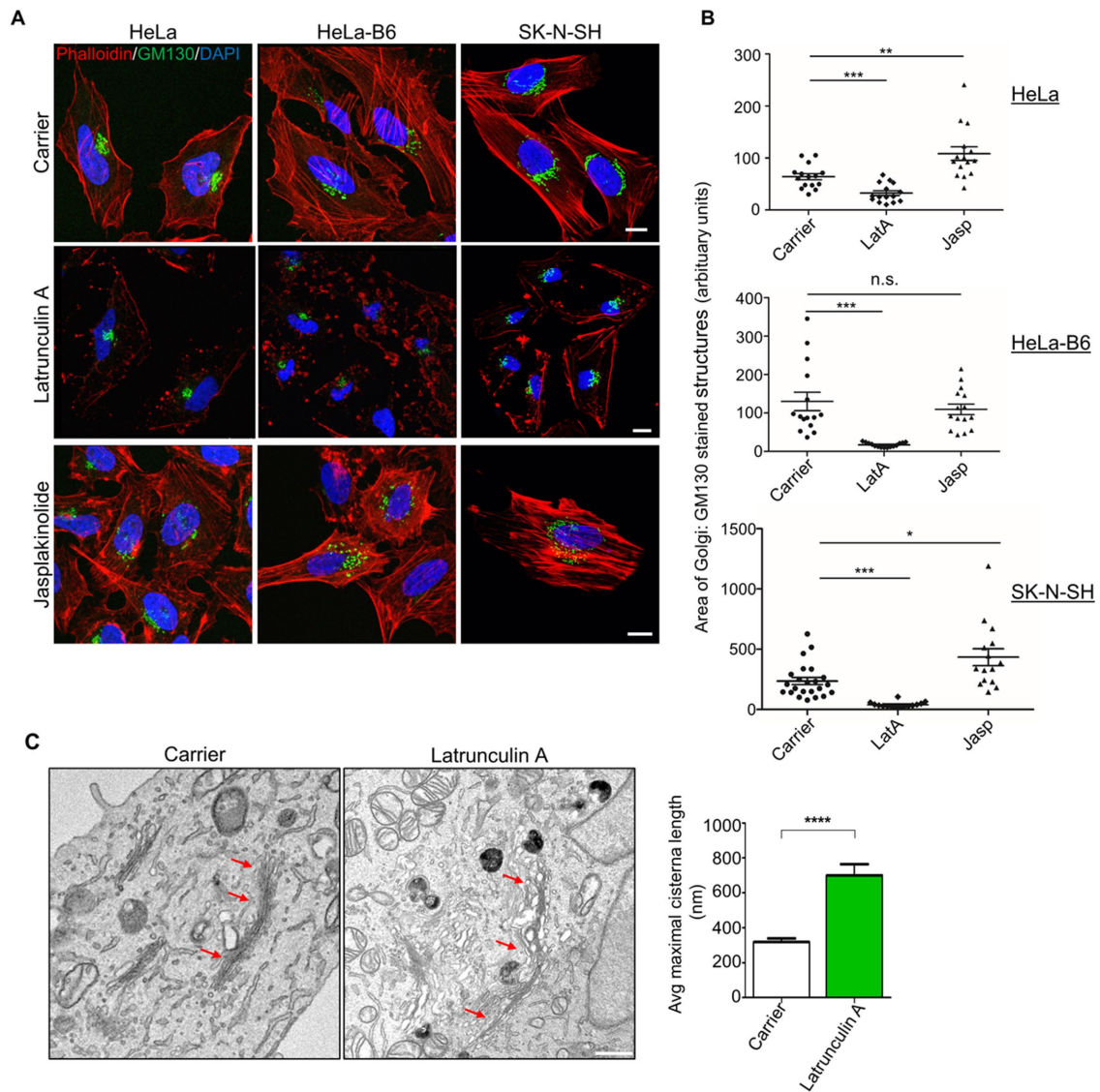


FIGURE 2: Perturbation of the Golgi ribbon by GCC88 is actin-dependent. (A) HeLa, HeLa-B6, and SK-N-SH cells were treated with either DMSO carrier, latrunculin A for 30 min, or jasplakinolide for 1 h, as indicated. Cells were then fixed and stained with phalloidin-TRITC (red) and mouse anti-GM130 (green) antibodies. Nuclei were stained with DAPI. Scale bars, 10 μ m. (B) Area of the Golgi defined by the Golgi marker, GM130, from cells treated with either DMSO carrier, latrunculin A, or jasplakinolide in A. Data from two independent experiments are pooled and expressed as the mean \pm SEM ($n = 15$) and analyzed by an unpaired, two-tailed Student's t test. * $p < 0.05$, ** $p < 0.01$, *** $p < 0.001$. (C) TEM of HeLa-B6 cells treated with either DMSO carrier or latrunculin A for 30 min. Cells were fixed in 1.5% GA and processed for electron microscopy as described. Quantitation of average cisternae length in HeLa-B6 treated with carrier or latrunculin A. Data are from >34 cells from each condition. Student's t test, mean \pm SEM, **** $p < 0.0001$. The arrows indicate the Golgi profiles in each section. Scale bar, 0.2 μ m.

in *Materials and Methods*. The classification of these proteins based on function is shown in a piechart (Figure 3B). The highest percentage of biotinylated proteins were those associated with membrane transport and the actin cytoskeleton. In view of the finding that the actin cytoskeleton was important in mediating the effects of GCC88 on the Golgi structure, we were particularly interested in these potential partners. There were four proteins identified associated with the actin cytoskeleton, namely EH domain Binding Protein 1 (EHBP), intersectin 1 (ITSN-1), ArfGAP with RhoGAP domain, Ankyrin repeat and PH Domain 1 (ARAP1), and Death-associated Inhibitor of Apoptosis 1 (DIAP1). Of the four biotinylated proteins, intersectin 1 (ITSN-1) was of particular interest as a

yeast two hybrid screen had previously detected an interaction between intersectin 1 and GCC88 (Wong *et al.*, 2012). ITSN-1 is a multi-domain protein with 2 Eps homology (EH) domains, five SH3 domains and a C-terminal Dbl (DH) homology domain, Peckstrin homology (PH) domain and C2 domain (Figure 3C). ITSN-1 coordinates actin assembly and is known to have a role in endocytosis (Hussain *et al.*, 2001; Herrero-Garcia and O'Bryan, 2017). ITSN-1 exists in two isoforms (Figure 3C), a long form containing the DH-PH-C2 domain at the C-terminus, a domain that has GEF activity for the Rho GTPase Cdc42, and a short form lacking the C-terminal DH-PH-C2 domain (Herrero-Garcia and O'Bryan, 2017). Eleven different ITSN-1 peptides were identified by MS in two independent experiments

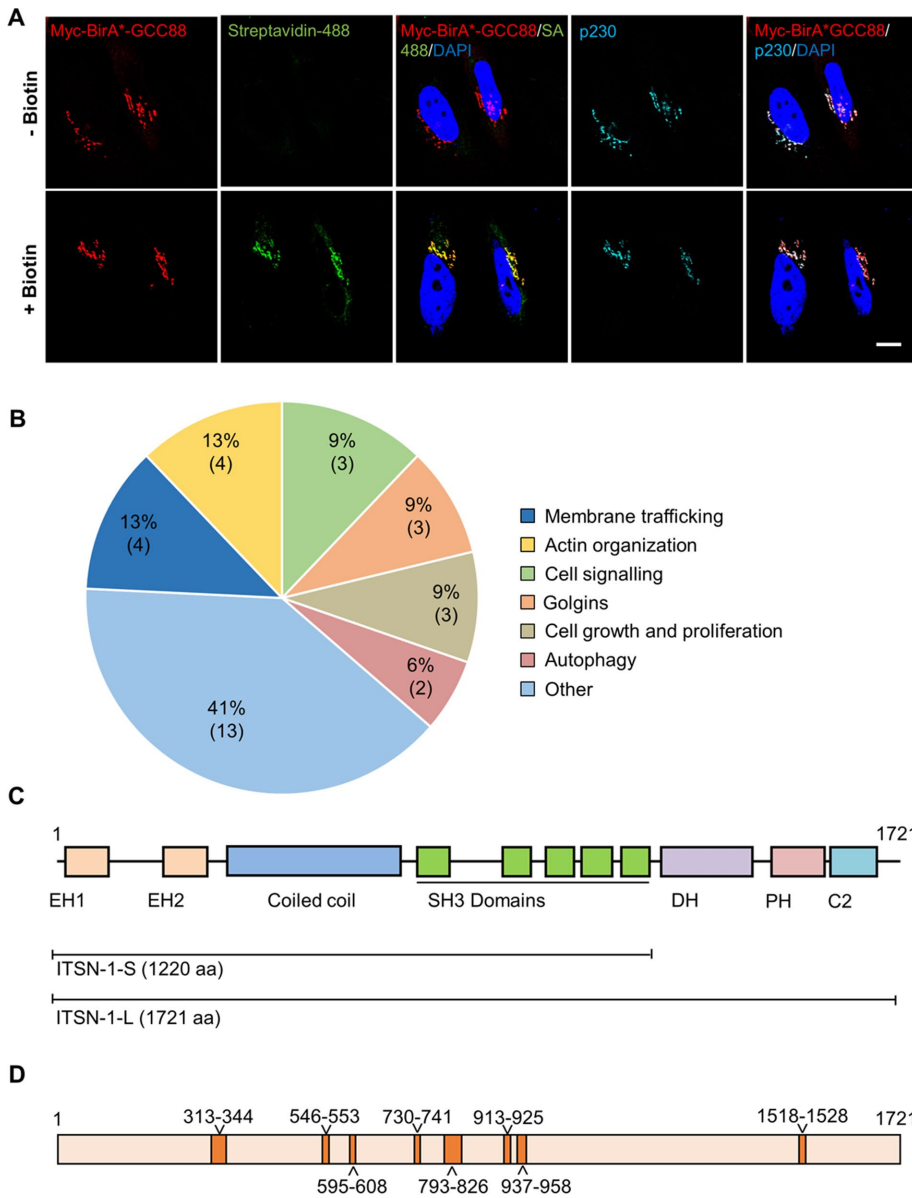


FIGURE 3: In vivo proximity-based labeling identified intersectin-1 as a candidate interactor of GCC88. (A) Parental HeLa cells transfected with Myc-BirA*-GCC88 were either left untreated or supplemented with 50 μ M biotin overnight and harvested 24 h after transfection. Monolayers were stained with mouse anti-Myc antibodies (red) and streptavidin Alexa Fluor 488 (green). Nuclei were stained using DAPI. Scale bar, 10 μ m. (B) Summary of the functional role of the proteins identified by MS using BioID. (C) Schematic representation of ITSN-1 domains. The short and long isoforms share the EH, coiled-coil, and SH3 domains, while the long isoform contains additional DH-PH-C2 domains, which confers GEF activity toward Cdc42. (D) The positions of the ITSN-1 peptides identified by MS analysis of biotinylated proteins. Peptides are derived from multiple regions of the ITSN-1 polypeptide with one peptide (1518–1528) belonging to the long isoform of ITSN-1. Some of the highlighted regions represent sequences from two distinct peptides identified in the analyses.

	Significant peptides (total)		Sequence coverage (%)		Protein score	
Experiment:	1	2	1	2	1	2
Intersectin-1	8	3	34.5	16.3	248	41

See Supplemental Appendix II for the identified peptide sequences, the mass/charge ratios, and the individual peptide and identity scores.

TABLE 1: Intersectin-1 peptides identified by MS in two BioID experiments: the number of significant peptides, the percent sequence coverage that all the peptides represent, and the protein score.

(Table 1 and Supplemental Appendix II); these peptides were derived from diverse regions of the 1721 residue long polypeptide including a peptide from the long isoform of ITSN-1 (Figure 3D). As the long form of ITSN-1 has not been previously reported in HeLa cells we analyzed HeLa cell extracts by immunoblotting and included extracts of primary neurons as a positive control, as neurons are known to have high levels of ITSN-1-L. Immunoblotting analyses revealed abundant levels of the 195-kDa ITSN-1-L species in neurons, as expected, whereas the 138-kDa short form of ITSN-1 was more abundant in HeLa cells. Significantly, low levels of the long form of ITSN-1 were also detected in HeLa cells (Supplemental Figure S3). Hence, both the short form and the long form of ITSN-1, the isoform that activates Cdc42, are present in HeLa cells, and from the BioID analysis, they both represent potential interaction partners of GCC88.

To directly determine whether there is a physical interaction between either isoform of ITSN-1 and GCC88, we performed a co-IP experiment using HeLa-B6 cells transiently transfected with either the long or the short isoform of FLAG-ITSN-1. In addition, we included FLAG-Rheb as a control. Antibodies to FLAG were used to immunoprecipitate the FLAG-tagged proteins from cell extracts and the immunoprecipitates were analyzed by immunoblotting. GFP-GCC88 was immunoprecipitated by both the short and long form of ITSN-1 but not with FLAG-Rheb (Figure 4A). These data demonstrate that both GCC88 and ITSN-1 are part of a complex.

We have previously shown that a construct with N-terminal deletion of GCC88 (Δ 1-279) is recruited to the Golgi but does not perturb the Golgi structure (Luke *et al.*, 2003). We assessed whether this truncation mutant was able to interact with ITSN-1 by IP from cells transfected with FLAG-ITSN-1 and Myc-GCC88 Δ 279. Whereas full length Myc-GCC88 was immunoprecipitated by FLAG-ITSN-1, the N-terminal truncation of GCC88 failed to be coprecipitated with FLAG-ITSN-1 (Supplemental Figure S4A). Neither the

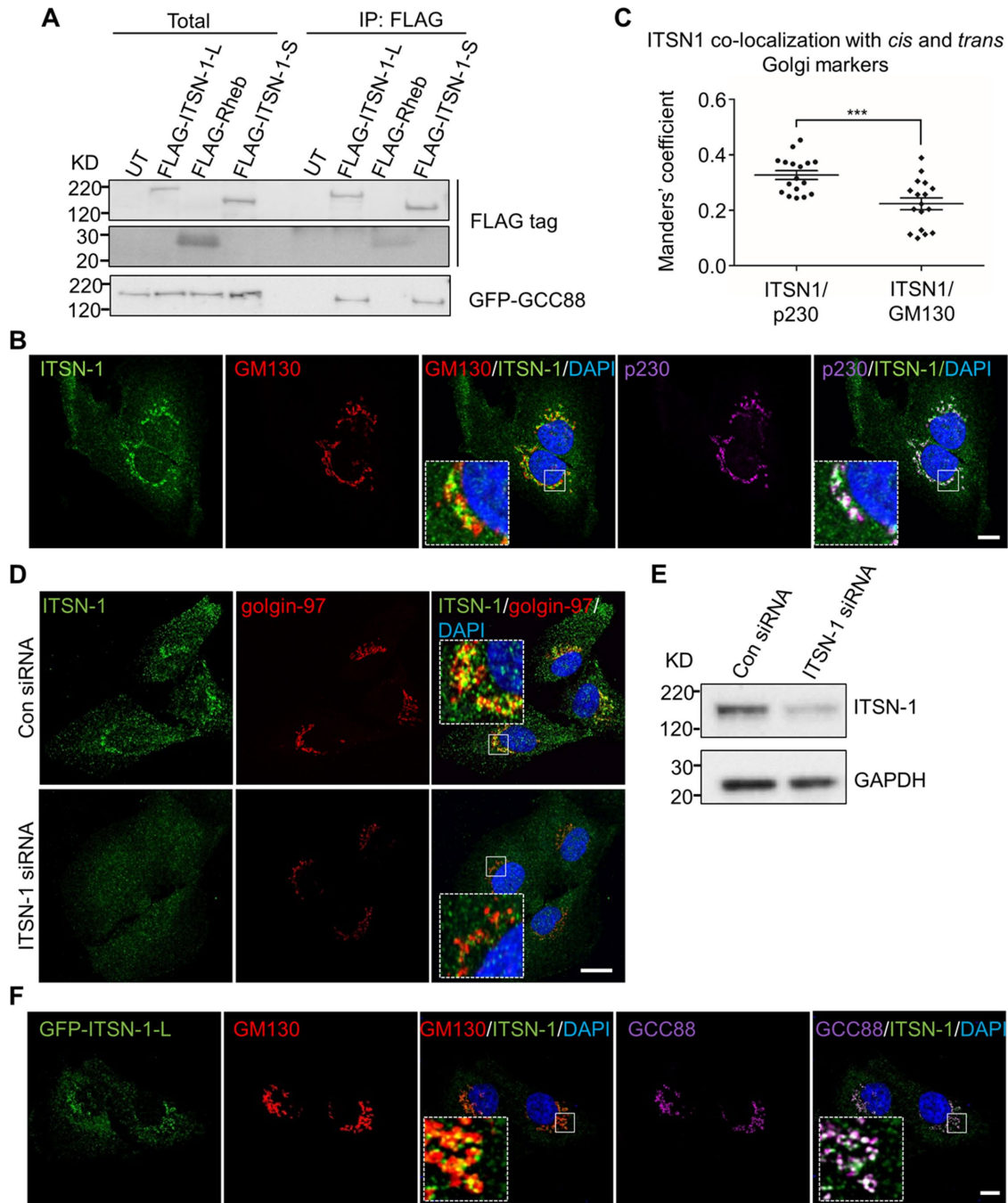


FIGURE 4: ITSN-1 interacts with GCC88 and localizes to the Golgi apparatus. (A) HeLa-B6 cell monolayers were transfected with FLAG-ITSN-1-L, FLAG-ITSN-1-S, or FLAG-Rheb as indicated. The cells were harvested and complexes containing the FLAG-tagged proteins were immunoprecipitated with anti-FLAG antibodies. Total cell extract (Total) and immunoprecipitate (IP) were analyzed by immunoblotting with mouse monoclonal anti-GFP or rabbit polyclonal anti-FLAG antibodies, as indicated, using a chemiluminescence detection system. Loadings represent approximately 5% of input and 30% of immunoprecipitate. (B) Immunostaining of SK-N-SH cells with rabbit anti-ITSN-1 (green), mouse anti-GM130 (red) (*cis*-Golgi marker), and human anti-p230/golgin-245 (magenta) antibodies. (C) Volocity software was used to calculate Manders' coefficient M1 values of ITSN-1 colocalization with the TGN marker p230/golgin-245 and with the *cis*-Golgi marker GM130. Data are presented as the mean \pm SEM from three independent experiments ($n = 17$) and analyzed by unpaired, two-tailed Student's *t* test. *** $p < 0.001$. (D, E) To confirm the specificity of the Golgi-localized signal using the ITSN-1 antibody, SK-N-SH cells were transfected with either control or ITSN-1 siRNA for 72 h. (D) Monolayers fixed and stained with rabbit anti-ITSN-1 (green) and mouse anti-golgin-97 (red) antibodies. Nuclei were stained using DAPI. (E) Cell extracts analyzed by immunoblotting with rabbit anti-ITSN-1 and mouse anti-GAPDH antibodies using a chemiluminescence detection system. (F) SK-N-SH cells were transiently transfected with GFP-ITSN-1-L for 24 h. Cells were fixed and stained with mouse anti-GM130 (red) and rabbit anti-GCC88 (magenta). Nuclei were stained using DAPI. Scale bars in B, D, and F, 10 μ m.

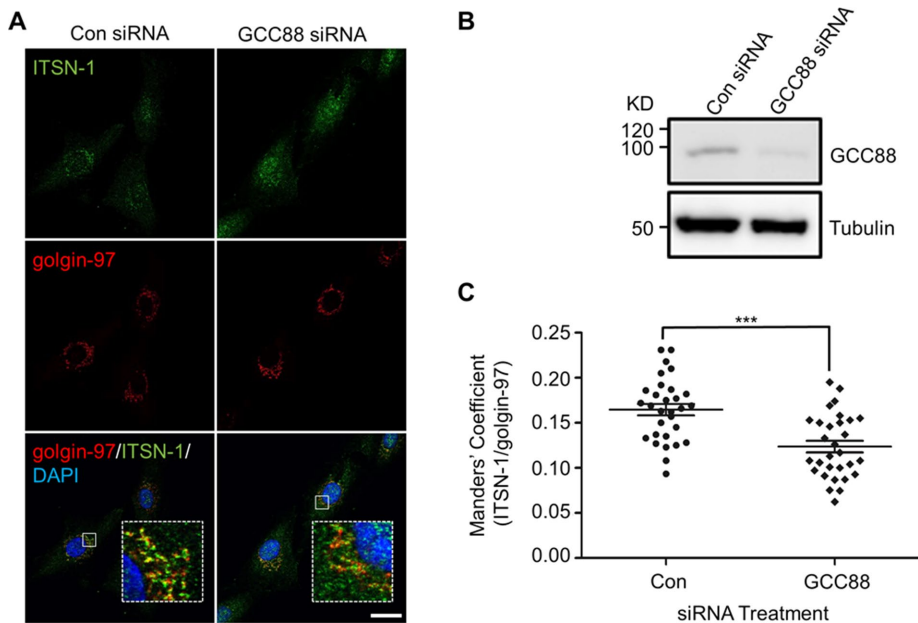


FIGURE 5: GCC88 contributes to the recruitment of ITSN-1 to the TGN. (A, B) SK-N-SH cells were transfected with either control or GCC88 siRNA for 72 h. (A) Monolayers were stained with rabbit anti-ITSN-1 (green) and mouse anti-golgin-97 (red) antibodies. Nuclei were stained with DAPI. Scale bar 10 μm . (B) Cell extracts were analyzed by immunoblotting using rabbit anti-GCC88 and mouse anti- α -tubulin to confirm the depletion of GCC88. (C) Quantitation of colocalization between ITSN-1 and golgin-97 using Manders' colocalization coefficient. $n = 30$ cells from three independent experiments. Data are represented as the mean \pm SEM. Student's t test, *** $p < 0.001$.

full-length Myc-GCC88 nor the GCC88 Δ 1-279 construct was co-precipitated with FLAG-Rheb (Supplemental Figure S4B). This finding demonstrates that the interaction between GCC88 and ITSN-1 correlates with the loss of the Golgi ribbon and supports the role of a GCC88-ITSN-1 interaction in regulating Golgi architecture.

Next, we determined whether ITSN-1 is located on the Golgi. SK-N-SH cells were used for these experiments, as endogenous ITSN-1 was readily detected by immunofluorescence in this cell line, in contrast to HeLa cells. Endogenous ITSN-1 in SK-N-SH showed both a perinuclear staining pattern and additional staining through the cytoplasm (Figure 4B). The perinuclear staining of ITSN-1 showed partial colocalization with the *cis*-Golgi marker GM130 and stronger colocalization with the TGN marker p230/golgin-245 (Figure 4B). Quantitation by the Manders coefficient showed a significant difference in the costaining of endogenous ITSN-1 with p230/golgin-245 as compared with GM130 (Figure 4C). Golgi staining with the anti-ITSN-1 antibody was abolished following silencing of ITSN-1 with small interfering RNA (siRNA) (Figure 4, D and E), demonstrating that the staining was specific. The antibodies used to detect endogenous ITSN-1 will detect both the short and long forms of ITSN-1. To determine whether the long form of ITSN-1, which includes the C-terminal GEF for Cdc42, can be localized to the Golgi, we expressed the GFP-ITSN-1-L in SK-N-SH cells. GFP-ITSN-1-L was partially localized to the Golgi, as demonstrated by colocalization with both the *cis* and TGN Golgi markers (Figure 4F). Line scan analyses of GFP-ITSN-1 fluorescence with the *cis*- and *trans*-Golgi markers revealed partial overlap between ITSN-1 and GM130 (Supplemental Figure S5A) and extensive overlap between ITSN-1 and GCC88 (Supplemental Figure S5B), indicating that ITSN-1 is localized to the TGN.

ITSN-1 is localized to the Golgi and enhances actin organization

To determine whether GCC88 is responsible for the Golgi localization of ITSN-1, we silenced endogenous GCC88 in SK-N-SH cells and assessed the extent of Golgi localization of ITSN-1 (Figure 5, A and B). Depletion of ITSN-1, which colocalized with the TGN marker golgin-97. Quantitation revealed a statistically significant reduction of 30% in the colocalization with the Golgi marker throughout the cell population (Figure 5C). On the other hand, total cell levels of ITSN-1 were not affected by GCC88 knockdown (Supplemental Figure S6A). Hence, GCC88 contributes to the recruitment of ITSN-1 to the Golgi, but is probably not the sole factor responsible for the total pool of ITSN-1 recruited to the Golgi.

To assess whether the interaction of GCC88 with ITSN-1 was promoting the altered Golgi phenotype in HeLa-B6 cells, we then silenced ITSN-1 in this cell clone. The fragmented Golgi phenotype of HeLa-B6 cells collapsed into a tight compact Golgi upon silencing ITSN-1 (Figure 6, A and C), whereas cells treated with control siRNA showed the typical fragmented Golgi of HeLa-B6 cells. Quantitation revealed that ~80% of the cells treated with ITSN-1 siRNA displayed a compact Golgi compared with ~20% in the control treated HeLa-B6 cells (Figure 6B). The level of GCC88 was similar in control and ITSN-1-depleted cells (Supplemental Figure S6B); thus the change in Golgi morphology is likely to be a direct consequence of a deficiency of ITSN-1. Hence, ITSN-1 directly contributes to the loss of the Golgi ribbon in cells overexpressing GCC88.

To assess whether elevated levels of ITSN-1 could influence the Golgi architecture, we examined the impact of overexpression of either the short or long form of ITSN-1 in HeLa cells. Overexpression of the long form of ITSN-1, but not the short form, in parental HeLa cells resulted in dispersal of the compact Golgi structure, as revealed by staining with both *cis*- and *trans*-Golgi markers (Figure 6D). The level of expression of the two isoforms of ITSN-1 was similar in these transfected cell populations (Figure 6E); moreover, the levels of either GCC88 (Figure 6E) or another golgin GM130 (Supplemental Figure S6C) in the transfected cell populations were similar to those in untransfected cells. These data indicate that the long form of ITSN-1, containing the GEF domain, is responsible for modulating Golgi architecture. In addition, staining with phalloidin showed an enhanced actin filament network in ITSN-1-L transfected cells compared with untransfected cells, showing that the long isoform of ITSN-1 was promoting actin assembly within these transfected cells (Figure 6F). These findings indicate a direct involvement of the long form of ITSN-1 in the maintenance of the Golgi structure.

To further analyze the ability of the short and long forms of ITSN-1 to influence Golgi morphology, we have also compared the ability of ITSN-1-L and ITSN-1-S to rescue the compact Golgi phenotype in HeLa-B6 cells depleted of total ITSN-1. The expression of FLAG-ITSN-1L in the ITSN-1 KD cells restored the fragmented Golgi phenotype of HeLa-B6 cells, whereas expression of

FLAG-ITSN-1S did not alter the compact Golgi in KD cell (Figure 6, G and H). Quantitation of the Golgi area (Figure 6I) clearly shows that FLAG-ITSN-1L expression dispersed the Golgi fragments, whereas the expression of FLAG-ITSN-1S had no impact on the compact Golgi. Hence these data further support the conclusion that the long isoform of ITSN-1, containing the Cdc42 GEF domain, is required for the altered morphology of the Golgi in HeLa-B6 cells.

Actin has been technically very difficult to visualize at the Golgi, probably due to the highly dynamic nature of the short actin filaments within the Golgi (Egea *et al.*, 2013). To attempt to demonstrate actin association with Golgi mini-stacks, we treated HeLa-B6 cells with LatA to depolymerize actin filaments and to compact the Golgi, and then washed out LatA and monitored the location of actin filaments using the RFP-utrophin calponin homology domain (UtrCH) in live cells over time. Whereas the Golgi in HeLa-B6 cells was compact after LatA treatment, as expected, within 40 min of LatA washout, GFP-GCC88-labeled Golgi fragments were observed that either costained with RFP-UtrCH or were in close proximity to the actin filaments (Supplemental Figure S7). These data show a correlation between actin polymerization around the Golgi and dispersal of Golgi fragments.

Role of nonmuscle myosin IIA in promoting actin-mediated Golgi fragmentation by GCC88

As actin assembly is important in the loss of the ribbon structure mediated by the TGN membrane tether GCC88, we reasoned that a myosin motor may be also necessary to provide the force necessary to drive the reorganization and dispersal of the Golgi membranes. p200/myosin II protein, analogous to nonmuscle myosin IIA heavy chain, has been reported to be located on the TGN and associated with TGN-derived membrane structures (Musch *et al.*, 1997; Stow and Heimann, 1998; Miserey-Lenkei *et al.*, 2010). Therefore, we assessed whether myosin IIA was required for loss of the Golgi ribbon in this system. Significantly, treatment of HeLa-B6 cells with blebbistatin, a specific inhibitor of nonmuscle myosin IIA, collapsed the Golgi fragments in a compact juxtanuclear location, whereas treatment with the myosin V inhibitor myoVin-1 had no effect (Figure 7A), as revealed by quantitation of Golgi area in these drug-treated cells (Figure 7B). These results indicate that myosin IIA may be the motor that promotes dispersal of Golgi membranes on actin filaments.

GCC88 is essential to pathways of Golgi fragmentation induced by alterations in membrane flux and by overexpression of tau

The architecture of the Golgi ribbon can be perturbed by a range of treatments and cell perturbations (Wei and Seemann, 2017). Dysregulation of either anterograde or retrograde membrane-transport pathways can result in Golgi fragmentation, considered to result from alterations in membrane flux through the Golgi. To determine whether the GCC88-actin pathway identified in this study is also relevant to other pathways of Golgi fragmentation, we silenced the retromer subunit Vps26, as the inhibition of retromer is known to affect multiple transport pathways from the early endosomes (Gallon and Cullen, 2015), including membrane flow into the TGN, resulting in extensive Golgi fragmentation (Seaman, 2004). Quantitation of cells following Vps26 siRNA treatment showed that 70% of Vps26 siRNA-treated cells had a dispersed Golgi and the remaining 30% of cells a compact Golgi (Figure 8, A and B; Supplemental Figure S8). We then asked whether dispersal of Golgi membrane arising from Vps26 knockdown required the presence of GCC88. In contrast, only 10% of cells treated with both GCC88 siRNA and

Vps26 siRNA showed a dispersed Golgi, whereas ~90% of cells had a compact Golgi (Figure 8, A and B; Supplemental Figure S8). Quantitation of the area of the Golgi, defined by the Golgi marker GM130, further confirmed that the double knockdown of GCC88 and Vps26 resulted in a more compact Golgi than the single knockdown of Vps26 (Figure 8C). Hence GCC88 is needed to promote Golgi dispersal following silencing of retromer, indicating that perturbation of the Golgi due to alterations in membrane flux requires the GCC88-ITSN-1 pathway.

Loss of the Golgi ribbon has been reported in a range of neurodegenerative diseases (Sundaramoorthy *et al.*, 2015), and there is evidence that Golgi fragmentation contributes to neuronal degradation in disease (Liu *et al.*, 2017a). We also investigated whether the GCC88-actin pathway is required for Golgi fragmentation in a model of neurodegeneration induced by overexpression of tau (Liazoghli *et al.*, 2005). Transfection of SK-N-SH neuroblastoma cells with GFP-Tau resulted in fragmentation of the Golgi in >80% of cells by 24 h posttransfection, whereas no (<10%) Golgi fragmentation was observed when GCC88 was silenced before expression of GFP-tau (Figure 8, D and E). Hence, the GCC88-ITSN-1 pathway is relevant to Golgi fragmentation initiated by different processes and pathways.

DISCUSSION

Defining the components that regulate the Golgi structure is pertinent to understanding how the morphology of the Golgi complex influences the regulation of a variety of higher-order functions (Gosavi and Gleeson, 2017; Wei and Seemann, 2017). In this study, we identified a novel molecular network at the TGN that couples to the actin cytoskeleton and regulates Golgi ribbon disassembly. We previously demonstrated that increased levels of the TGN golgin GCC88 lead to the loss of the Golgi ribbon and its dispersal into Golgi mini-stacks, and that the loss of the compact Golgi ribbon resulted in reduced mTORC1 activity and an increase in autophagy (Gosavi *et al.*, 2018). A question arising from this earlier finding was the identity of the mechanism by which GCC88 was driving a change in Golgi structure. Here we have identified the protein scaffold ITSN-1 as a novel TGN component and a GCC88 binding partner that links the Golgi complex to the actin cytoskeleton to regulate Golgi structure. The novel GCC88-ITSN-1 pathway described in this report is important in regulating the dynamics of the Golgi structure in multiple processes leading to dispersal and/or fragmentation of the Golgi ribbon, including Golgi fragmentation mediated by changes in membrane flux and tau-overexpression.

ITSN-1 is a highly conserved scaffold protein found in a range of organisms (Hunter *et al.*, 2013). ITSN has been studied mainly for its role in endocytosis, as ITSN-1 is known to interact with components of the endocytic machinery. However, other studies, including a yeast two-hybrid screen, identified a large number of additional binding partners (Wong *et al.*, 2012), suggesting that this scaffold molecule could be involved in a range of other pathways. Vertebrates have two ITSN genes, ITSN-1 and ITSN-2, each giving rise to two isoforms. The longer isoforms include an extension at the C-terminus of the short isoform with additional domains that have GEF activity for Cdc42 (Gubar *et al.*, 2013; Hunter *et al.*, 2013), a GTPase that regulates the actin network. Overexpression of the C-terminal domains of ITSN-1-L promotes actin polymerization (Hussain *et al.*, 2001), demonstrating a role for the long isoform in actin assembly. Of potential relevance to the current study is that the long isoform, which promotes actin polymerization, is absent in invertebrates, organisms that do not have a Golgi ribbon (Hunter *et al.*, 2013; Gosavi and Gleeson, 2017). ITSN-1-L is particularly enriched in neuronal

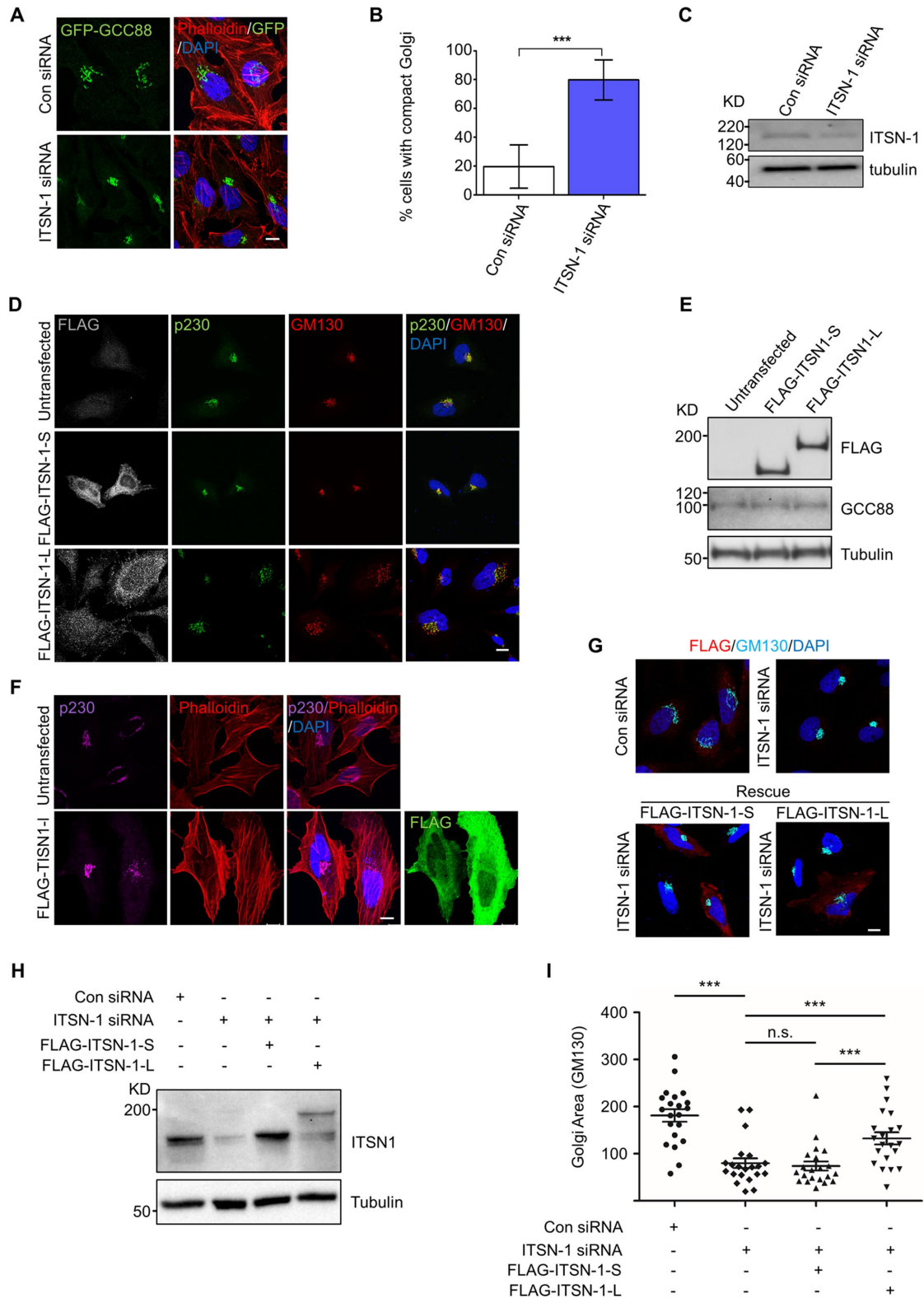


FIGURE 6: Effect of silencing and overexpression of ITSN-1 on Golgi architecture. (A–C) Silencing of ITSN-1 compacts the Golgi in HeLa-B6 cells. HeLa-B6 cells transfected with control siRNA or ITSN-1 siRNA for 72 h and monolayers stained with phalloidin-TRITC antibodies (red). Nuclei were stained with DAPI. (A) ITSN-1 silencing restored the juxtannuclear tight Golgi staining pattern. Nuclei were stained with DAPI. (B) The Golgi staining patterns of 64 cells from three independent experiments were scored. Mean \pm SD, *** p < 0.001 by Student's t test. (C) Cell extracts from A were analyzed by immunoblotting using rabbit anti-ITSN-1 and mouse anti- α -tubulin antibodies. (D) Immunostaining of untransfected HeLa cells or HeLa cells transfected with either FLAG-ITSN-1-S or FLAG-ITSN-1-L for 24 h with mouse anti-GM130 (red), rabbit anti-FLAG (gray), and human anti-p230 (green) antibodies. (E) Cell extracts from untransfected HeLa cells or HeLa cells transfected with either FLAG-ITSN-1-S or FLAG-ITSN-1-L were analyzed by immunoblotting

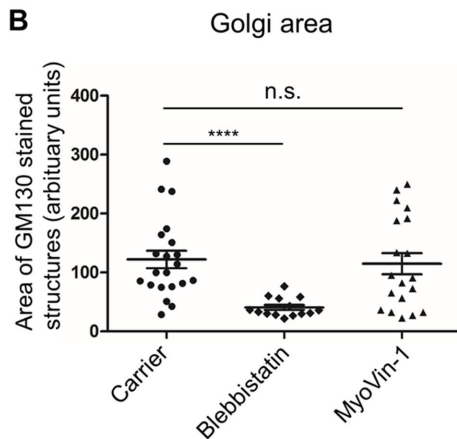
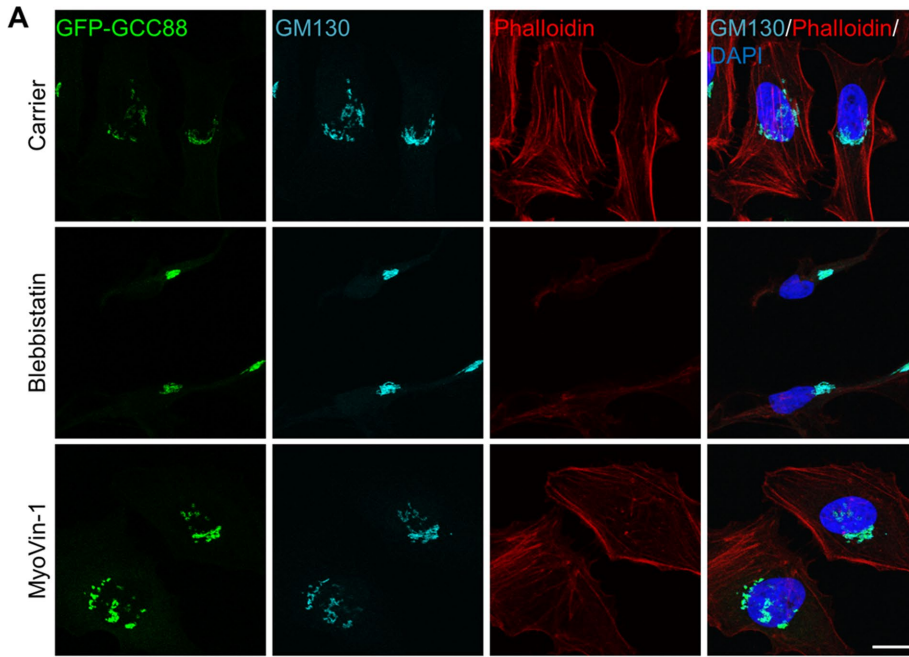


FIGURE 7: Effect of inhibitors of myosins on compact structure of the Golgi in HeLa-B6 cells. (A) HeLa B6 cells were treated with 50 μ M blebbistatin or 10 μ M myoVin-1 for 1.5 h before fixing and then stained with phalloidin-TRITC (red) and mouse anti-GM130 (cyan) antibodies. Nuclei were stained with DAPI. Scale bar, 10 μ m. (B) Area of the Golgi defined by the Golgi marker, GM130, from A. Data are pooled from two independent experiments and expressed as the mean \pm SEM ($n > 13$) and analyzed by an unpaired, two-tailed Student's *t* test. **** $p < 0.0001$, n.s. not significant.

cells, and there have been a number of studies exploring the role of the long isoform in neuronal functions (Irie and Yamaguchi, 2002; Yu et al., 2008). Here we demonstrate, by immunoblotting and MS analysis, that low levels of ITSN-1-L are also present in HeLa cells,

highlighting a role for the long isoform of ITSN-1 in nonneuronal cells. Importantly, the ITSN peptides identified by MS were all unique to ITSN-1 and not related to the ITSN-2 sequence. Moreover, we have demonstrated that ITSN-1 was responsible for the loss of the Golgi ribbon mediated by overexpression of GCC88, as 1) silencing of ITSN-1 rescued the Golgi phenotype in HeLa-B6 cells, 2) overexpression of ITSN-1-L but not of ITSN-1-S promoted Golgi fragmentation, 3) silencing GCC88 reduces the ITSN-1 pool at the Golgi, and 4) a truncated form of GCC88 that does not promote Golgi fragmentation (Luke et al., 2003) also does not bind to ITSN-1. Collectively, the data strongly suggest that the long isoform of ITSN-1 is responsible for mediating the changes in Golgi architecture arising from increased levels of GCC88. However, at this stage, we cannot discount the possibility that the short form of ITSN-1 also contributes to Golgi architecture in this system.

A previous report identified a small molecule (ZCL278) that inhibited Cdc42-GEF binding, based on the interaction with ITSN-1 in vitro, thereby inhibiting Cdc42 function; ZCL278 disrupted Golgi morphology, suggesting an ITSN1-like GEF interaction with Cdc42 at the Golgi (Friesland et al., 2013). However, the responsible Cdc42-GEF at the Golgi was not identified by Friesland et al. (2013). Our findings provide definitive evidence that the long form of ITSN-1, which contains a GEF for Cdc42, is located at the TGN.

The evidence that ITSN-1L is a binding partner of GCC88 is supported by the following observations. First, ITSN-1L was identified as a partner/near neighbor of GCC88 in vivo by the BioID/MS analysis. Second, FLAG-tagged ITSN-1L coimmunoprecipitated GFP-tagged and Myc-tagged GCC88, whereas another FLAG-tagged Golgi protein did not coimmunoprecipitate GCC88. Third, an N-terminal truncation of GCC88 failed to be coprecipitated with FLAG-ITSN-1, demonstrating that the interaction is specific. Fourth, endogenous GCC88 and ITSN-1L are both localized at the TGN. Finally, depletion of GCC88 resulted in a reduction of ITSN-1 at the TGN. Attempts to coimmunoprecipitate endogenous GCC88 and ITSN-1L were not successful, most likely

using rabbit anti-FLAG, rabbit anti-GCC88, and mouse anti- α tubulin antibodies. (F) Immunostaining of untransfected HeLa cells or HeLa cells transfected with FLAG-ITSN-1-L and stained with phalloidin-TRITC (red), rabbit anti-FLAG (green), and human anti-p230 (magenta) antibodies. (G-I) Expression of FLAG-ITSN-1-S or FLAG-ITSN-1-L constructs (+Rescue) in ITSN-1 siRNA-treated HeLa-B6 cells. HeLa-B6 cells were treated with control siRNA or ITSN-1 siRNA for 72 h or for 48 h and then transfected with either FLAG-ITSN-1-S or FLAG-ITSN-1-L, as indicated, for a further 24 h. (G) Monolayers were then stained with mouse anti-GM130 (blue) and rabbit anti-FLAG antibodies (red). Nuclei were stained with DAPI. (H) Cell extracts were analyzed by immunoblotting using rabbit anti-ITSN-1 and mouse anti- α tubulin antibodies. (I) Area of the Golgi defined by the Golgi marker GM130 from G. Data are pooled from two independent experiments and expressed as the mean \pm SEM. Each symbol represents an individual cell. Data were analyzed by an unpaired, two-tailed Student's *t* test. *** $p < 0.001$, n.s. not significant. Scale bars in A, D, F, and G, 10 μ m.

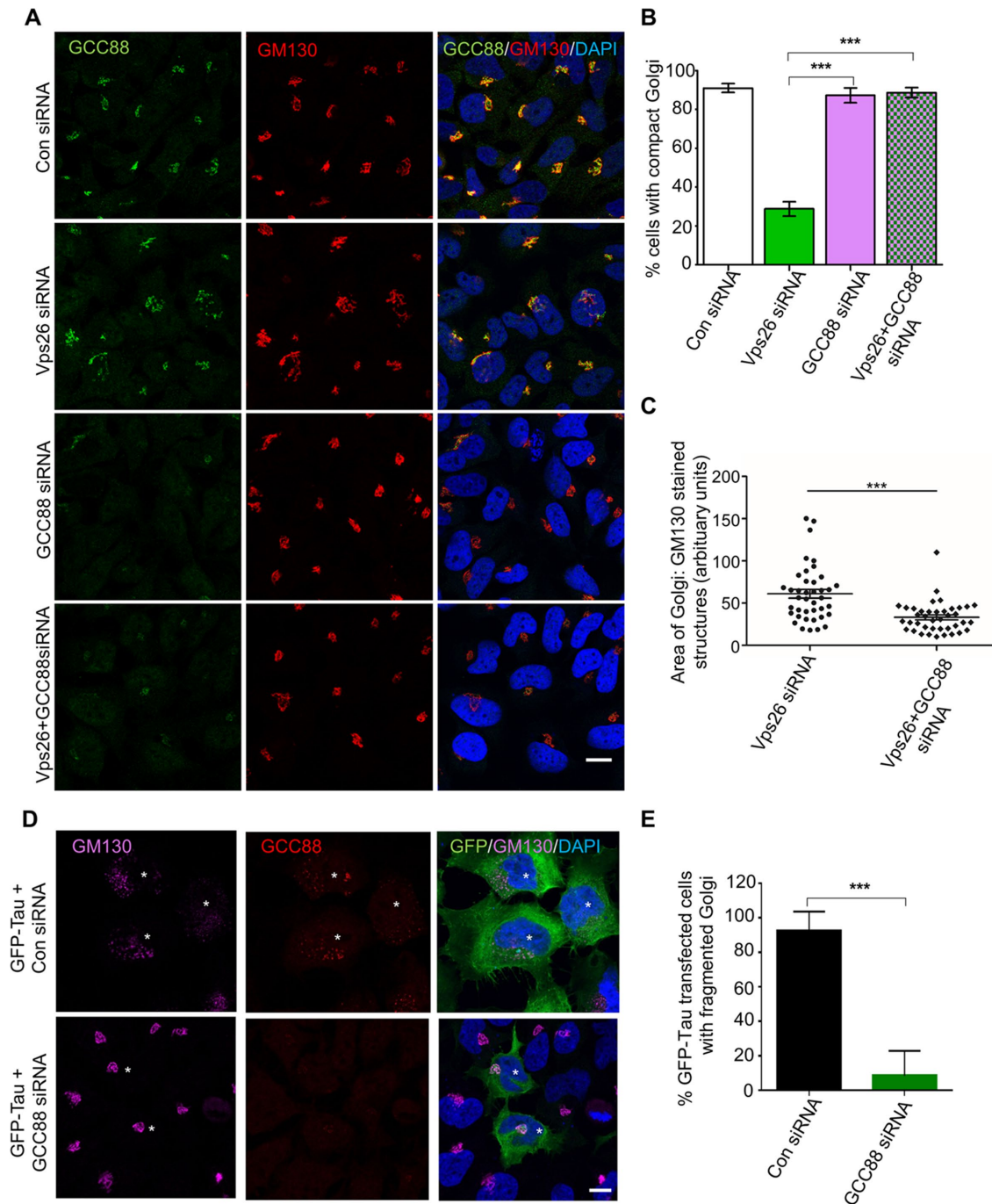


FIGURE 8: GCC88 is required for the Golgi fragmentation phenotype induced by different pathways. (A, B, C) GCC88 is required for Golgi fragmentation induced by depletion of retromer. (A) Parental HeLa cells were transfected with control, Vps26, GCC88, or both Vps26 and GCC88 siRNA for 72 h. Cells were fixed and stained with rabbit anti-GCC88 (green) and mouse anti-GM130 (red). Scale bar, 20 μ m. (B) The Golgi staining patterns of >200 cells from four independent experiments were scored. Mean \pm SEM, *** p < 0.001 by Student's t test. (C) Area of the Golgi defined by the Golgi marker GM130, from A. Data from two independent experiments are pooled, expressed as the mean \pm SEM (n = 40), and analyzed by an unpaired, two-tailed Student's t test. *** p < 0.001. (D, E) GCC88 is required for Golgi fragmentation induced by overexpression of tau. (D) SK-N-SH cells were transfected with control or GCC88 siRNA for 48 h and then transfected again with GFP-tau for 24 h. Cells were then fixed and stained for GM130 (magenta) and GCC88 (red). Nuclei were stained with DAPI. Asterisks indicate GFP-tau transfected cell. Scale bar, 10 μ m. (E) The Golgi staining pattern of >25 GFP-tau-positive cells from two independent experiments were scored. Mean \pm SEM, *** p < 0.001 by Student's t test.

due to low levels of ITSN-1L in HeLa cells and limitations of the sensitivity of the anti-ITSN-1 antibody. Nonetheless, collectively, our data strongly support an interaction between GCC88 and ITSN-1L.

The long form of ITSN-1 is known to activate the small GTPase, Cdc42, and distinct pools of Cdc42 have been identified in various locations, including the Golgi complex (Erickson *et al.*, 1996;

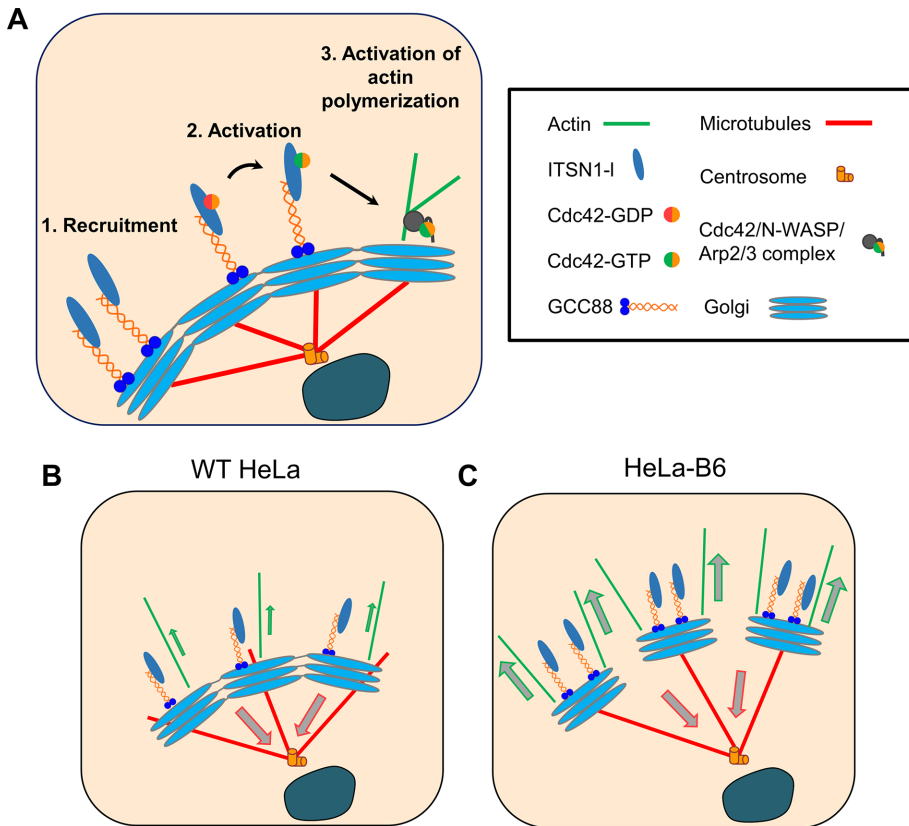


FIGURE 9: Model of the regulation of the Golgi ribbon by the GCC88-ITSN-1 pathway. (A) The data presented in this manuscript show that GCC88 binds and recruits ITSN-1-L to the TGN. The long form of ITSN has GEF activity for Cdc42. We propose that activated Cdc42 at the TGN promotes actin nucleation, possibly via the interaction of Cdc42 with WASP and the Arp2/3 complex. (B, C) The model depicting the impact of increased (different) levels of GCC88 at the TGN on Golgi architecture. The level of GCC88 at the TGN regulates the recruitment of ITSN-1-L and the extent of actin polymerization. (B) The situation in parental HeLa cells; (C) HeLa-B6 cells with increased levels of GCC88. The balance of the outward forces generated by the actinomyosin cytoskeleton and the inward forces generated by the dynein-MT system would then define the status of the Golgi architecture in a tug-of-war. Elevated levels of GCC88, C, would promote, via enhanced recruitment of ITSN-1-L, an increase in the F-actin network at the TGN and an increase in actinomyosin forces, resulting in reduction/loss of the compact Golgi ribbon.

Michaelson *et al.*, 2001; Farhan and Hsu, 2016). Hence, Golgi-localized ITSN-1-L could directly activate Cdc42 to promote actin polymerization. Indeed, we have shown here that the loss of the Golgi ribbon mediated by GCC88 is an actin-dependent process. Treatment of HeLa-B6 cells with LatA, an inhibitor of F-actin assembly, resulted in the restoration of a compact Golgi and a ribbon structure. Other studies have also shown that LatA treatment of wild-type HeLa cells results in a more compact Golgi; however, by EM, the Golgi structure was highly disorganized with swollen cisternae (Lazaro-Dieguez *et al.*, 2006). The LatA treatments in our study were considerably shorter than in these other reports, which probably accounts for the intact ribbon we observed after drug treatment. On the other hand, stabilization of actin filaments with jasplakinolide resulted in Golgi fragmentation of the compact ribbon in parental HeLa and SK-N-SH cells. There are a number of other examples that demonstrate that actin, independent of microtubules, is involved in maintaining the structural integrity of the Golgi ribbon (Gosavi and Gleeson, 2017), and our work here further reinforces the importance of actin in regulating the Golgi structure. Actin has previously been shown to facilitate the formation of the

Golgi ribbon, mediated by the Golgi stacking protein GRASP65. GRASP65 is required for both the formation of stable Golgi stacks and ribbon linking, and the latter function is mediated by the binding partner of GRASP, Mena, an actin elongation factor that promotes actin polymerization (Tang *et al.*, 2016). Our work describes a role for actin independent of GRASP65 and involving a process located at the TGN. We were able to observe actin polymerization in close proximity to the Golgi fragments of HeLa-B6 cells during LatA washout experiments, but attempts to directly visualize actin associated with the Golgi mini-stacks in HeLa-B6 cells under steady state conditions, using fluorescent actin probes, were not successful. However, this was not unexpected, given that actin has been technically very difficult to visualize at the Golgi. The difficulty in visualizing actin may be due to the presence of short actin filaments associated with Golgi membranes (Percival *et al.*, 2004).

Actin has been shown to be important in the generation of transport carriers at the TGN (Dippold *et al.*, 2009; Miserey-Lenkei *et al.*, 2010; Guet *et al.*, 2014), and furthermore, the mechanism by which the actin cytoskeleton promotes membrane tubulation for the biogenesis of transport carriers is now emerging (Anitei and Hoflack, 2011; Guet *et al.*, 2014). Our data show that actin is also important at the TGN in regulating the Golgi ribbon structure. How actin regulates two distinct membrane processes, transport carrier biogenesis and changes in Golgi architecture at the TGN, is not clear at this stage. Indeed, compared with the generation of transport carriers, the mechanism(s) by which actin regulates the structural integrity and architecture of the Golgi complex is currently very poorly

understood. The latter function may reflect the precise organization of the GCC88 membrane tethers within a subdomain of the TGN.

On the basis of our findings in this study, we propose that GCC88-ITSN-1 interaction is important in coupling actin polymerization at the TGN to negatively regulate the length of the Golgi ribbon. We propose that GCC88 recruits ITSN-1-L to the TGN, which in turn activates Cdc42 at the *trans*-face of the Golgi (Figure 9A). Activated Cdc42 could then promote actin nucleation at the TGN, possibly via the known interactions of Cdc42 with WASP and the Arp2/3 complex (Hussain *et al.*, 2001; Humphries *et al.*, 2014). In support of a role for Cdc42 in this model are the location of a pool of Cdc42 at the Golgi (Erickson *et al.*, 1996; Michaelson *et al.*, 2001; Farhan and Hsu, 2016) and the observation that a small molecule inhibitor of the Cdc42-ITSN interaction perturbs Golgi organization (Friesland *et al.*, 2013). The nonmuscle myosin IIA, which we demonstrated to be required for the phenotype in HeLa-B6 cells and which is known to be associated with TGN membranes (Musch *et al.*, 1997; Stow and Heimann, 1998; Miserey-Lenkei *et al.*, 2010), could then provide the motor force to pull out Golgi membranes

along actin filaments. The balance of the outward forces generated by the actin cytoskeleton and the inward forces generated by the dynein–MT system would then define the status of the Golgi architecture in a tug-of-war. Elevated levels of GCC88 would promote, via enhanced recruitment of ITSN-1-L, an increase in the F-actin network at the TGN and an increase in actinomyosin forces, resulting in loss of the compact Golgi ribbon (Figure 9B). On the other hand, reduced levels of GCC88 would reduce actin-mediated outward forces, allowing the dynein motor forces along microtubules to dominate, resulting in a compact and elongated ribbon structure. Indeed, depletion of GCC88 (Gosavi *et al.*, 2018) or ITSN-1 (this study) resulted in an enhanced ribbon structure compared with that in parental HeLa cells. The relevance of these architectural modifications of the Golgi to various cell pathways is highlighted by our previous finding that mTORC1 signaling is dramatically reduced in HeLa-B6 cells (Gosavi *et al.*, 2018), suggesting that the changes in architecture are accompanied by changes in Golgi membrane components responsible for recruitment of mTOR.

The Golgi architecture varies in different cell types, from a very compact juxtannuclear Golgi ribbon to a more dispersed distribution that extends from the perinuclear region. Neurons, for example, have Golgi mini-stacks dispersed into the dendrites (Hanus and Ehlers, 2008), and it is of interest that both GCC88 and ITSN are more highly expressed in neurons than in many other cells (www.proteinatlas.org/), including HeLa cells. Hence, the findings in this paper raise the possibility that the distinct morphology of the Golgi in different cell types may reflect the levels of GCC88 and ITSN-1.

Fragmentation of the Golgi ribbon occurs under a variety of conditions, including perturbations in membrane flux into and out of the Golgi and neurodegeneration. Our finding that GCC88 is required for the Golgi fragmentation arising from perturbations of membrane flux by silencing retromer and by the induction of Golgi fragmentation following tau overexpression emphasizes the important role of the GCC88-ITSN-1-L network in pathways involving loss of the Golgi ribbon. Golgi fragmentation is associated with a number of neurodegenerative diseases, and it is of interest that ITSN-1 has been reported to be very highly expressed in the brains of individuals with Alzheimer's disease (Herrero-Garcia and O'Bryan, 2017), raising the possibility that the F-actin pathway we have discovered could be relevant to the pathology associated with this neurodegenerative disease. Hence, this novel GCC88-ITSN-1 pathway, which is coupled to F-actin, may have broad significance in pathophysiological processes.

MATERIALS AND METHODS

Cell culture and transfection

Mycoplasma-free authentic HeLa cells (Curie Institute, Paris) and SK-N-SH cells (American Type Culture Collection [ATCC], Manassas, VA) were maintained as semiconfluent monolayers in DMEM (Thermo Fisher Scientific, Australia), and CHO cells (ATCC, Manassas, VA) were maintained in Roswell Park Memorial Institute (RPMI) medium supplemented with 10% (vol/vol) fetal bovine serum (FBS; GibcoLife Technologies, Australia), 2 mM L-glutamine, 100 U/μl penicillin, and 0.1% (wt/vol) streptomycin (complete DMEM) in a humidified 10% CO₂ atmosphere at 37°C. HeLa-B6 cell clone (Gosavi *et al.*, 2018) was maintained in the presence of 1 mg/ml G418 (Thermo Fisher Scientific, Australia).

Transient transfections of fusion protein constructs were performed using FuGENE 6 transfection reagent (Promega, USA), Lipofactamine 2000, or Lipofactamine 3000 (Thermo Fisher Scientific, Australia) according to the manufacturer's protocol.

Mouse primary cortical neuronal cultures were generated as described by Toh *et al.* (2018) and maintained in neurobasal medium supplemented with 2.5% B-27, 0.25% GlutaMAX, and 100 U/μl penicillin and 0.1% streptomycin (complete NBMs; Life Technologies, USA). Cells were grown for 7–14 d before transduction with lentivirus.

Plasmids, antibodies, and reagents

Constructs encoding GFP-full-length GCC88, Myc-tagged GCC88, and Myc-GCC88ΔN1-279 have been described previously (Luke *et al.*, 2003). FLAG-Intersectin-1 short (human; Addgene plasmid # 47392), FLAG-Intersectin-1 long (human; Addgene plasmid # 47393), and GFP-intersectin-1 long (human; Addgene plasmid # 47395) were a gift from Peter McPherson (McGill University; Hussain *et al.*, 2001). pcDNA3-FLAG-Rheb was a gift from Fuyuhiko Tamanoi (UCLA Molecular Biology Institute; Addgene plasmid # 19996; Urano *et al.*, 2007). pRK5-EGFP-Tau was a gift from Karen Ashe (University of Minnesota; Addgene plasmid # 46904; Hoover *et al.*, 2010). psPAX2 was a gift from Didier Trono (École Polytechnique Fédérale Lausanne; Addgene plasmid # 12260), pFUGW-H1 empty vector a gift from Sally Temple (Neural Stem Cell Institute, New York; Addgene plasmid # 25870; Fasano *et al.*, 2007), and pCMV-VSV-G a gift from Bob Weinberg (Whitehead Institute for Biomedical Research; Addgene plasmid # 8454; Stewart *et al.*, 2003). pcDNA3.1 Myc-BioID was a gift from Kyle Roux (South Dakota State University; Addgene plasmid # 35700) (Roux *et al.*, 2012) and pCS2.0 Tag-RFP-T-UtrCH was a gift from Alpha Yap (University of Queensland; Addgene plasmid # 101279) (Wu *et al.*, 2014). To generate Myc-BirA*-GCC88 fusion protein, GCC88 cDNA was amplified from Myc-GCC88 (Luke *et al.*, 2003) as one fragment (bases 1–2328) using the primers CGGAATTCATGGAGAAGTTTGGGATGAA and CGCGGATCCTCATCTCTTGCC AGAAGG. The PCR product was subcloned into the *EcoRI*/*Bam*HI sites of pcDNA3.1 mycBioID. Primers were designed to amplify the region of interest and to introduce *EcoRI* or *Bam*HI sites at the 5' and 3' ends. The PCR products were digested with *EcoRI* and *Bam*HI and cloned into the *EcoRI* and *Bam*HI sites of pcDNA3.1 Myc-BioID, which resulted in the fusion of BirA* to the N-terminus of the protein of interest. Biotin (Sigma Aldrich) was reconstituted in DMEM at a concentration of 1 mM and was used at a final concentration of 50 μM.

Rabbit polyclonal antibodies to human GCC88 have been described (Luke *et al.*, 2003). Mouse monoclonal antibodies to human golgin-97 (#CDF4 A-21270, 1:600) and GM130 (#610882, 1:600) were purchased from BD Biosciences (Australia). Mouse monoclonal antibodies to ITSN-1 (ABS984, 1:1000) were purchased from Merck (Australia). Human autoantibodies to p230 have been described (Kooy *et al.*, 1992). Mouse monoclonal antibodies to GAPDH were purchased from Calbiochem (#MAP374, 1:5000). Rabbit polyclonal antibodies to Vps26 (#ab23892, 1:200) and Myc tag (9B11; #ab9106, 1:2000) were purchased from Abcam (UK). Mouse monoclonal antibody to Myc-Tag (9B11; #2276S, 1:1000) were purchased from NEB (USA). Mouse monoclonal antibody to α-tubulin (clone DM1A, 1:5000) and rabbit polyclonal antibodies to FLAG (#F7425 1:2000) were obtained from Sigma-Aldrich. Phalloidin–tetramethylrhodamine B isothiocyanate (phalloidin–TRITC) P1951 (Sigma-Aldrich) was used to detect actin filaments. Mouse monoclonal antibodies to GFP (clone 7.1 and 17.1, #11814460001, 1:1000) were purchased from Roche Applied Science (Germany).

Secondary antibodies used for immunofluorescence were goat anti-rabbit immunoglobulin G (IgG)-Alexa Fluor 568 nm, goat anti-mouse IgG-Alexa Fluor 568 nm, goat anti-rabbit IgG-Alexa Fluor 488 nm, goat anti-mouse IgG-Alexa Fluor 488 nm, goat anti-mouse

IgG-Alexa Fluor 647 nm, goat anti-rabbit IgG-Alexa Fluor 647 nm, and goat anti-human Alexa Fluor 568 or 647 nm were from Life Technologies (Grand Island, NY). All secondary antibodies were used at the dilution 1:500. Horseradish peroxidase-conjugated rabbit anti-goat Ig, horseradish peroxidase-conjugated sheep anti-rabbit Ig, and anti-mouse Ig were from DAKO Corporation (Carpentaria, CA). Streptavidin-Alexa Fluor 488 and streptavidin-horseradish peroxidase were purchased from Life Technologies.

Generation of GFP-GCC88 lentivirus and transduction of primary neurons

pFUGW-H1-GFP-GCC88 was generated from full-length GCC88 (Luke *et al.*, 2003). Recombinant lentivirus was produced by transfection of HEK293T cells with pCMV-VSV-G, psPAX2, and pFUGW-H1-GFP-GCC88 or pFUGW-H1 (empty vector) as described by Dull *et al.* (1998). Virus was collected and precipitated with PEG-it (Integrated Sciences) and resuspended in DMEM containing HEPES. Cultures of mouse cortical neurons (7 d old) were transduced with recombinant lentivirus for 6 d before fixation and staining.

RNA interference

Transfections with siRNA were performed using DharmaFECT1 siRNA transfection reagent (GE Lifesciences/Millennium Science, Victoria, Australia) according to the manufacturer's instructions for 72 h before analysis. Human GCC88 was targeted with the specific siRNA 5'-GUCAGCAAUCUCAGGUAGA-3' (Lieu *et al.*, 2007), and human Vps26 siRNA (5'-CTCTATTAAGATGGAAGTG-3') has been previously described (Arighi *et al.*, 2004). Human ITSN-1 was targeted with the specific siRNA 5'CUAAUUAUGUAAAGCUUCU[dTdT] 3'. All duplex siRNAs, including a control siRNA, were synthesized by Sigma-Aldrich (Australia).

Indirect immunofluorescence

Monolayers on coverslips were fixed with 4% (vol/vol) paraformaldehyde (PFA) for 15 min, followed by quenching in 50 mM NH₄Cl/phosphate-buffered saline (PBS) for 10 min. Cells were permeabilized in 0.1% Triton X-100 in PBS for 4 min and incubated in 5% FBS in PBS for 20 min to reduce nonspecific binding. Monolayers were incubated with primary and secondary conjugates as described (Kjer-Nielsen *et al.*, 1999), with the exception that monolayers stained with rabbit anti-ITSN-1 were fixed and quenched, washed twice with 0.2% Triton X-100 in PBS, and blocked in 2% BSA/0.2% Triton X-100 in PBS for 30 min. Monolayers were then incubated with primary antibody, diluted in 2% BSA/0.2% Triton X-100 in PBS for 1 h, washed in 0.2% Triton X-100 in PBS, and incubated with secondary conjugates for 40 min. Monolayers were stained with 4',6 diamidino-2-phenylindole (DAPI) for 5 min, washed in PBS, and finally rinsed with MilliQ before being mounted in Mowiol.

Confocal microscopy and image analysis

Images were acquired using a laser confocal scanning microscope (Leica LCS SP8 confocal imaging system) using a 63 × 1.4 NA HCX PL APO CS oil immersion objective. GFP and Alexa Fluor 488 were excited with the 488-nm line of an argon laser, Alexa Fluor 568 with a 543-nm HeNe laser, Alexa Fluor 647 with a 633-nm HeNe laser, and DAPI with a 405-nm UV laser. Images were collected sequentially for multicolor imaging. Fluorescence images for each experiment were collected using identical settings. Volocity 6.3 (Perkin Elmer-Cetus) imaging software was used for Manders' colocalization coefficient analysis in the entire cell with automatic thresholding (Costes *et al.*, 2004). Quantitation was carried out for the indicated number of cells.

Line spectrum reports were generated for a region of interest using LAS X Life Science microscope software and exported into Excel, which was used to construct the line graphs.

The area of the Golgi was measured by manual demarcation, defined by GM130 stained structures, with a limiting polygon and calculation of its area using ImageJ (Farber-Katz *et al.*, 2014).

Live cell imaging

Monolayers of HeLa-B6 cells were transfected with RFP-T-UtrCH using FuGENE 6 transfection reagent according to the manufacturer's protocol and incubated for 24 h. Coverslips were mounted in a round chamber and placed on the microscope stage. Cells were incubated in C-DMEM (Life Technologies) containing 1.25 μM latrunculin A for 25 min; the drug was then washed out and the cells were imaged in C-DMEM for 40 min to monitor actin filament regeneration. Time-lapse acquisitions were performed at 37°C using a thermostat-controlled stage and an Inverted Eclipse Ti-E (Nikon) microscope equipped with a CSU-W1 spinning disk confocal head (Andor) and an iXon Ultra (EM-CCD) camera (Andor). Z-stacks were captured every 2 min using Metamorph software (Molecular Devices).

Immunoblotting

Cells were lysed in RIPA buffer (1 mM Tris/Cl, pH 7.5, 15 mM NaCl, 0.5 mM EDTA, 0.01% SDS, 0.1% Triton X-100, and 0.1% deoxycholate) containing protease inhibitors (Sigma-Aldrich, Australia). Aliquots of the extracts were added to reducing SDS sample buffer and boiled for 5 min at 100°C. Proteins were resolved by SDS-PAGE using 4–12% NuPAGE gels and transferred onto Immobilon-P polyvinylidene fluoride (PVDF) membrane (Millipore, Australia) at 30 V overnight at 4°C. The membrane was blocked by drying at 37°C. The membrane was incubated with antibodies diluted in 10% (wt/vol) milk/PBS, either at room temperature for 1 h or overnight at 4°C, and then washed three times, each for 10 min, in 0.1% (vol/vol) PBS-Tween 20. The PVDF membrane was then incubated with horseradish peroxidase-conjugated secondary antibodies, diluted in 10% (wt/vol) milk/PBS for 1 h, and washed as above. Bound antibodies were detected by enhanced chemiluminescence (Amersham, GE Healthcare, Australia) and captured using the Gel-Pro Analyzer version 4.5 software (MediaCybernetics, Bethesda, MD) or the Chemi-Doc MP imager system (Bio-Rad).

Electron microscopy

Cells were fixed by adding freshly prepared 2% wt/vol PFA and 1.5% glutaraldehyde (Electron Microscopy Sciences) in 0.1 M sodium cacodylate buffer (pH 7.4) to an equal volume of culture medium for 5 min, followed by postfixation in the same buffer at 4°C overnight. Ultrathin sections of 100 nm were cut using a Leica Ultramicrotome UC7 and stained as described (Deerinck *et al.*, 2010). Images were acquired on an FEI Tecnai F20 at 200 kV with a HAADF detector.

Drug treatments

Cells were treated with drugs diluted in complete DMEM for the indicated time periods and fixed in 4% PFA before proceeding to immunostaining. Dimethyl sulfoxide (DMSO) (0.05–0.2%) was used as a carrier control for all drug treatments. Cells were treated with 10 μM nocodazole (Sigma) at 37°C for up to 2 h, 1 μM latrunculin A (Calbiochem) at 37°C for 30 min, 1 μM jasplakinolide (Calbiochem) at 37°C for 1 h, 10 μM myoVin-1 (Calbiochem) at 37°C for 1.5 h, and 50 μM blebbistatin (Abcam) at 37°C for 1.5 h.

BioID

BioID was carried out using HeLa cells in (4–6) × 100 mm tissue culture plates per sample, with the following modifications from the method described (Roux *et al.*, 2013). HeLa cells (~1.0 × 10⁶) were seeded into each plate and after 24 h were transiently transfected with 3–4.5 µg DNA (Myc-BirA* or Myc-BirA*-GCC88) per plate. The medium was supplemented with 50 µM sterile filtered biotin (Sigma Aldrich, USA) in c-DMEM (Life Technologies) for a period of 16–20 h and the cells harvested 24 h after transfection by scraping in 5 mM EDTA/PBS. Cells were pelleted at 1400 rcf, 4°C for 5 min, washed with PBS, and lysed in Lysis buffer (1% [vol/vol] Triton X-100 and 1× complete Mini EDTA-free protease inhibitor cocktail [Sigma Aldrich] in PBS) for 30 min on ice. Tris-Cl/PBS (50 mM) was added after the lysis at a 1:1 ratio and the cell debris was pelleted by centrifugation at 16,500 × g at 4°C for 10 min. Cell lysates were incubated overnight with NeutrAvidin agarose resin (Thermo Scientific) on a rotator at 4°C. The beads were washed once with wash buffer 1 (0.1% [wt/vol] sodium deoxycholate, 1% Triton X-100, 1 mM EDTA, 500 mM NaCl, and 50 mM HEPES in MilliQ water), a second time with wash buffer 2 (0.5% [wt/vol] sodium deoxycholate, 0.5% IGPAL CA-630, 1 mM EDTA, 250 mM LiCl, and 10 mM Tris-Cl, pH 7.4 in MilliQ water), and a final wash was performed in PBS.

Mass spectrometry

An in-gel trypsin digest protocol was used to prepare samples for analysis by mass spectrometry. Bands were excised by taking sections along the full length of the gel and were destained with multiple volumes of 50% (vol/vol) acetonitrile in 25 mM triethylammonium bicarbonate (TEAB). The gel fragments were dehydrated with 100% acetonitrile and reduced in 10 mM *tris* 2-carboxyethylphosphine (TCEP) made up in 50 mM triethylammonium bicarbonate (TEAB) for 1 h at 60°C. Proteins were then alkylated in the dark with 55 mM iodoacetamide in 50 mM TEAB for 30–60 min. Samples were then dehydrated in 100% acetonitrile, allowed to dry, and then incubated overnight with 0.25 µg trypsin (Sigma) at 37°C. Trypsin digests were centrifuged and the supernatant was transferred into tubes containing 1 µl 25% formic acid.

Samples were analyzed on a LTQ Orbitrap Elite (Thermo Scientific) coupled to an Ultimate 3000 RSLC nanosystem (Dionex). The nanoLC system was equipped with an Acclaim Pepmap nanotrap column and an Acclaim Pepmap analytical column. The peptide mix (2 µl) was loaded onto the trap column at 3% acetonitrile containing 0.1% formic acid for 5 min before the enrichment column was switched in line with the analytical column. The LC gradient was 3–25% acetonitrile over 20 min and then 40% acetonitrile for 2 min (total run time was 38 min). The LTQ Orbitrap Elite mass spectrometer was operated in the data-dependent mode; spectra were acquired first in positive mode at 240k resolution followed by collision-induced dissociation (CID) fragmentation. Twenty of the most intense peptide ions with charge states ≥2 were isolated per cycle and fragmented using a normalized collision energy of 35 and an activation Q of 0.25 (CID).

Analysis of proteomics data

Data analysis was carried out using the Mascot protein identification search engine (Matrix Science, v2.4) and restricted to the SWIS-SPROT database. Search parameters used were 10-ppm peptide mass tolerance and 0.6-Da fragment ion mass tolerance. Carbamidomethyl (C) was set as a fixed modification and variable modifications were included: oxidation (M), biotin (K), and biotin (N-term). Three missed cleavages were permitted and the search taxonomy was restricted to *Homo sapiens*. Peptides with mascot ion scores

greater than the homology score were considered significant. Proteins identified in the Myc-BirA* control were subtracted from the Myc-BirA*-GCC88 sample and proteins were filtered further in the Myc-BirA*-GCC88 sample to contain at least three unique peptide matches. A protein was designated as a candidate interactor of GCC88 if it exclusively appeared in at least two independent experiments.

Statistical analyses

Quantitation of the colocalization was performed using Volocity imaging software (Perkin Elmer, UK). Quantitation was carried out for the indicated number of cells at each time point. All analyses included samples from two or more independent experiments. Data are expressed as mean ± SEM or mean ± SD, as indicated, and analyzed by an unpaired, two-tailed Student's *t* test. *p* < 0.05 (*) was considered significant, *p* < 0.01 (**) was highly significant, and *p* < 0.001 (***) and *p* < 0.0001 (****) were very highly significant. The absence of a *p*-value indicates that the differences were not significant (n.s.).

ACKNOWLEDGMENTS

Confocal microscopy was performed at the Biological Optical Microscopy Platform (BOMP) at the University of Melbourne. This work was supported by funding from the Australian Research Council (DP100102394). We gratefully acknowledge Fiona Houghton for reagents, technical advice, and suggestions and Lou Fourrière-Chea for expert advice on live imaging.

REFERENCES

- Anitei M, Hoflack B (2011). Bridging membrane and cytoskeleton dynamics in the secretory and endocytic pathways. *Nat Cell Biol* 14, 11–19.
- Arighi CN, Hartnell LM, Aguilar RC, Haft CR, Bonifacino JS (2004). Role of the mammalian retromer in sorting of the cation-independent mannose 6-phosphate receptor. *J Cell Biol* 165, 121–133.
- Brandizzi F, Barlowe C (2013). Organization of the ER–Golgi interface for membrane traffic control. *Nat Rev Mol Cell Biol* 14, 381–392.
- Brownhill K, Wood L, Allan V (2009). Molecular motors and the Golgi complex: staying put and moving through. *Semin Cell Dev Biol* 20, 781–792.
- Bubb MR, Spector I, Beyer BB, Fosen KM (2000). Effects of jasplakinolide on the kinetics of actin polymerization. An explanation for certain *in vivo* observations. *J Biol Chem* 275, 5161–5170.
- Buschman MD, Xing M, Field SJ (2015). The GOLPH3 pathway regulates Golgi shape and function and is activated by DNA damage. *Front Neurosci* 9, 362.
- Colanzi A, Suetterlin C, Malhotra V (2003). Cell-cycle-specific Golgi fragmentation: how and why? *Curr Opin Cell Biol* 15, 461–467.
- Copeland SJ, Thurston SF, Copeland JW (2016). Actin- and microtubule-dependent regulation of Golgi morphology by FHDC1. *Mol Biol Cell* 27, 261–276.
- Costes SV, Daelemans D, Cho EH, Dobbin Z, Pavlakis G, Lockett S (2004). Automatic and quantitative measurement of protein–protein colocalization in live cells. *Biophys J* 86, 3991–4003.
- Coue M, Brenner SL, Spector I, Korn ED (1987). Inhibition of actin polymerization by latrunculin A. *FEBS Lett* 213, 311–318.
- De Matteis MA, Mironov AA, Beznoussenko GV (2008). *The Golgi Ribbon and the Function of the Golgins*, Springer-Verlag/Wein: New York.
- Deerinck TJ, Bushong EA, Thor A, Ellisman MH (2010). NCIMR methods for 3D EM: a new protocol for preparation of biological specimens for serial block face scanning electron microscopy. *Nat Center Microsc Imag Res* 6–8.
- Dippold HC, Ng MM, Farber-Katz SE, Lee SK, Kerr ML, Peterman MC, Sim R, Wiharto PA, Galbraith KA, Madhavarapu S, *et al.* (2009). GOLPH3 bridges phosphatidylinositol-4-phosphate and actomyosin to stretch and shape the Golgi to promote budding. *Cell* 139, 331–351.
- Dull T, Zufferey R, Kelly M, Mandel RJ, Nguyen M, Trono D, Naldini L (1998). A third-generation lentivirus vector with a conditional packaging system. *J Virol* 72, 8461–8471.
- Egea G, Serra-Peinado C, Salcedo-Sicilia L, Gutierrez-Martinez E (2013). Actin acting at the Golgi. *Histochem Cell Biol* 140, 341–360.

- Erickson JW, Zhang C, Kahn RA, Evans T, Cerione RA (1996). Mammalian Cdc42 is a brefeldin A-sensitive component of the Golgi apparatus. *J Biol Chem* 271, 26851–26854.
- Farber-Katz SE, Dippold HC, Buschman MD, Peterman MC, Xing M, Noakes CJ, Tat J, Ng MM, Rahajeng J, Cowan DM, et al. (2014). DNA damage triggers Golgi dispersal via DNA-PK and GOLPH3. *Cell* 156, 411–427.
- Farhan H, Hsu VW (2016). Cdc42 and cellular polarity: emerging roles at the Golgi. *Trends Cell Biol* 26, 241–248.
- Farhan H, Rabouille C (2011). Signalling to and from the secretory pathway. *J Cell Sci* 124, 171–180.
- Fasano CA, Dimos JT, Ivanova NB, Lowry N, Lemischka IR, Temple S (2007). shRNA knockdown of Bmi-1 reveals a critical role for p21-Rb pathway in NSC self-renewal during development. *Cell Stem Cell* 1, 81–99.
- Friesland A, Zhao Y, Chen YH, Wang L, Zhou H, Lu Q (2013). Small molecule targeting Cdc42-intersectin interaction disrupts Golgi organization and suppresses cell motility. *Proc Natl Acad Sci USA* 110, 1261–1266.
- Gallon M, Cullen PJ (2015). Retromer and sorting nexins in endosomal sorting. *Biochem Soc Trans* 43, 31–47.
- Glick BS, Nakano A (2009). Membrane traffic within the Golgi apparatus. *Annu Rev Cell Dev Biol* 25, 111–132.
- Gonatas NK, Stieber A, Gonatas JO (2006). Fragmentation of the Golgi apparatus in neurodegenerative diseases and cell death. *J Neurol Sci* 246, 21–30.
- Gosavi P, Gleeson PA (2017). The function of the Golgi ribbon structure—an enduring mystery unfolds! *Bioessays* 39, doi: 10.1002/bies.201700063.
- Gosavi P, Houghton FJ, McMillan PJ, Hanssen E, Gleeson PA (2018). The Golgi ribbon in mammalian cells negatively regulates autophagy by modulating mTOR activity. *J Cell Sci* 131, jcs211987.
- Goud B, Gleeson PA (2010). TGN golgins, Rabs and cytoskeleton: regulating the Golgi trafficking highways. *Trends Cell Biol* 20, 321–336.
- Gubar O, Morderer D, Tsyba L, Croise P, Houy S, Ory S, Gasman S, Rynditch A (2013). Intersectin: the crossroad between vesicle exocytosis and endocytosis. *Front Endocrinol (Lausanne)* 4, 109.
- Guet D, Mandal K, Pinot M, Hoffmann J, Abidine Y, Sigaut W, Bardin S, Schauer K, Goud B, Manneville JB (2014). Mechanical role of actin dynamics in the rheology of the Golgi complex and in Golgi-associated trafficking events. *Curr Biol* 24, 1701–1711.
- Hanus C, Ehlers MD (2008). Secretory outposts for the local processing of membrane cargo in neuronal dendrites. *Traffic* 9, 1431–1445.
- Herrero-Garcia E, O'Bryan JP (2017). Intersectin scaffold proteins and their role in cell signaling and endocytosis. *Biochim Biophys Acta* 1864, 21–30.
- Hoover BR, Reed MN, Su J, Penrod RD, Kotilinek LA, Grant MK, Pitstick R, Carlson GA, Lanier LM, Yuan LL, et al. (2010). Tau mislocalization to dendritic spines mediates synaptic dysfunction independently of neurodegeneration. *Neuron* 68, 1061–1081.
- Humphries AC, Donnelly SK, Way M (2014). Cdc42 and the Rho GEF intersectin-1 collaborate with Nck to promote N-WASP-dependent actin polymerisation. *J Cell Sci* 127, 671–685.
- Hunter MP, Russo A, O'Bryan JP (2013). Emerging roles for intersectin (ITSN) in regulating signaling and disease pathways. *Int J Mol Sci* 14, 7821–7852.
- Hussain NK, Jenna S, Glogauer M, Quinn CC, Wasiak S, Guipponi M, Antonarakis SE, Kay BK, Stossel TP, Lamarche-Vane N, McPherson PS (2001). Endocytic protein intersectin-1 regulates actin assembly via Cdc42 and N-WASP. *Nat Cell Biol* 3, 921–932.
- Irie F, Yamaguchi Y (2002). EphB receptors regulate dendritic spine development via intersectin, Cdc42 and N-WASP. *Nat Neurosci* 5, 1111–1118.
- Kjer-Nielsen L, van Vliet C, Erlich R, Toh BH, Gleeson PA (1999). The Golgi-targeting sequence of the peripheral membrane protein p230. *J Cell Sci* 112, 1641–1654.
- Kooy J, Toh BH, Pettitt JM, Erlich R, Gleeson PA (1992). Human autoantibodies as reagents to conserved Golgi components—characterization of a peripheral, 230-kDa compartment-specific Golgi protein. *J Biol Chem* 267, 20251–20263.
- Kupfer A, Dennert G, Singer SJ (1983). Polarization of the Golgi apparatus and the microtubule-organizing center within cloned natural killer cells bound to their targets. *Proc Natl Acad Sci USA* 80, 7221–7228.
- Lazaro-Dieguez F, Jimenez N, Barth H, Koster AJ, Renau-Piqueras J, Llopis JL, Burger KN, Egea G (2006). Actin filaments are involved in the maintenance of Golgi cisternae morphology and intra-Golgi pH. *Cell Motil Cytoskeleton* 63, 771–791.
- Liazoghli D, Perreault S, Micheva KD, Desjardins M, Leclerc N (2005). Fragmentation of the Golgi apparatus induced by the overexpression of wild-type and mutant human tau forms in neurons. *Am J Pathol* 166, 1491–1514.
- Lieu ZZ, Derby MC, Teasdale RD, Hart C, Gunn P, Gleeson PA (2007). The Golgin, GCC88, is required for efficient retrograde transport of cargo from the early endosomes to the trans-Golgi network. *Mol Biol Cell* 18, 4971–4991.
- Liu C, Mei M, Li Q, Roboti P, Pang Q, Ying Z, Gao F, Lowe M, Bao S (2017a). Loss of the golgin GM130 causes Golgi disruption, Purkinje neuron loss, and ataxia in mice. *Proc Natl Acad Sci USA* 114, 341–351.
- Liu J, Yang X, Li B, Wang J, Wang W, Liu J, Liu Q, Zhang X (2017b). STK16 regulates actin dynamics to control Golgi organization and cell cycle. *Sci Rep* 7, 44607.
- Lowe M (2011). Structural organization of the Golgi apparatus. *Curr Opin Cell Biol* 23, 81–93.
- Luini A, Parashuraman S (2016). Signaling at the Golgi: sensing and controlling the membrane fluxes. *Curr Opin Cell Biol* 39, 31–42.
- Luke MR, Kjer-Nielsen L, Brown DL, Stow JL, Gleeson PA (2003). GRIP domain-mediated targeting of two new coiled-coil proteins, GCC88 and GCC185, to subcompartments of the trans-Golgi network. *J Biol Chem* 278, 4211–4226.
- Mayinger P (2011). Signaling at the Golgi. *Cold Spring Harb Perspect Biol* 3.
- McKinnon CM, Mellor H (2017). The tumor suppressor RhoBTB1 controls Golgi integrity and breast cancer cell invasion through METTL7B. *BMC Cancer* 17, 145.
- Michaelson D, Silletti J, Murphy G, D'Eustachio P, Rush M, Philips MR (2001). Differential localization of Rho GTPases in live cells: regulation by hypervariable regions and RhoGDI binding. *J Cell Biol* 152, 111–126.
- Millarte V, Farhan H (2012). The Golgi in cell migration: regulation by signal transduction and its implications for cancer cell metastasis. *Scientific-WorldJournal* 2012, 498278.
- Miserey-Lenkei S, Chalancon G, Bardin S, Formstecher E, Goud B, Echard A (2010). Rab and actomyosin-dependent fission of transport vesicles at the Golgi complex. *Nat Cell Biol* 12, 641–654.
- Munro S (2011). The golgin coiled-coil proteins of the Golgi apparatus. *Cold Spring Harb Perspect Biol* 3, a005256.
- Musch A, Cohen D, Rodriguezboulant E (1997). Myosin II is involved in the production of constitutive transport vesicles from the TGN. *J Cell Biol* 138, 291–306.
- Nelson WJ (2000). W(h)ither the Golgi during mitosis? *J Cell Biol* 149, 241–248.
- Percival JM, Hughes JA, Brown DL, Schevzov G, Heimann K, Vrhovski B, Bryce N, Stow JL, Gunning PW (2004). Targeting of a tropomyosin isoform to short microfilaments associated with the Golgi complex. *Mol Biol Cell* 15, 261–280.
- Rabouille C, Haase G (2015). Editorial: Golgi pathology in neurodegenerative diseases. *Front Neurosci* 9, 489.
- Ramirez IB, Lowe M (2009). Golgins and GRASPs: holding the Golgi together. *Semin Cell Dev Biol* 20, 771–779.
- Rios RM, Borens M (2003). The Golgi apparatus at the cell centre. *Curr Opin Cell Biol* 15, 61–66.
- Roux KJ, Kim DI, Burke B (2013). BioID: a screen for protein-protein interactions. *Curr Protoc Protein Sci* 74, Unit 19 23.
- Roux KJ, Kim DI, Raida M, Burke B (2012). A promiscuous biotin ligase fusion protein identifies proximal and interacting proteins in mammalian cells. *J Cell Biol* 196, 801–810.
- Sanders AA, Kaverina I (2015). nucleation and dynamics of Golgi-derived microtubules. *Front Neurosci* 9, 431.
- Scott KL, Kabbarah O, Liang MC, Ivanova E, Anagnostou V, Wu J, Dhakal S, Wu M, Chen S, Feinberg T, et al. (2009). GOLPH3 modulates mTOR signalling and rapamycin sensitivity in cancer. *Nature* 459, 1081–1090.
- Seaman MN (2004). Cargo-selective endosomal sorting for retrieval to the Golgi requires retromer. *J Cell Biol* 165, 111–122.
- Short B, Haas A, Barr FA (2005). Golgins and GTPases, giving identity and structure to the Golgi apparatus. *Biochim Biophys Acta* 1744, 381–395.
- Spector I, Shochet NR, Kashman Y, Groweiss A (1983). Latrunculins: novel marine toxins that disrupt microfilament organization in cultured cells. *Science* 219, 491–495.
- Stewart SA, Dykxhoorn DM, Palliser D, Mizuno H, Yu EY, An DS, Sabatini DM, Chen IS, Hahn WC, Sharp PA, et al. (2003). Lentivirus-delivered stable gene silencing by RNAi in primary cells. *RNA* 9, 491–501.

- Stow JL, Heimann K (1998). Vesicle budding on Golgi membranes: regulation by G proteins and myosin motors. *Biochim Biophys Acta* 1404, 161–171.
- Sundaramoorthy V, Sultana JM, Atkin JD (2015). Golgi fragmentation in amyotrophic lateral sclerosis, an overview of possible triggers and consequences. *Front Neurosci* 9, 400.
- Sutterlin C, Colanzi A (2010). The Golgi and the centrosome: building a functional partnership. *J Cell Biol* 188, 621–628.
- Tang D, Zhang X, Huang S, Yuan H, Li J, Wang Y (2016). Mena-GRASP65 interaction couples actin polymerization to Golgi ribbon linking. *Mol Biol Cell* 27, 131–152.
- Toh WH, Chia PZC, Hossain MI, Gleeson PA (2018). GGA1 regulates signal-dependent sorting of BACE1 to recycling endosomes, which moderates A β production. *Mol Biol Cell* 29, 191–208.
- Urano J, Sato T, Matsuo T, Otsubo Y, Yamamoto M, Tamanoi F (2007). Point mutations in TOR confer Rheb-independent growth in fission yeast and nutrient-independent mammalian TOR signaling in mammalian cells. *Proc Natl Acad Sci USA* 104, 3511–3519.
- Wei JH, Seemann J (2010). Unraveling the Golgi ribbon. *Traffic* 11, 1391–1400.
- Wei JH, Seemann J (2017). Golgi ribbon disassembly during mitosis, differentiation and disease progression. *Curr Opin Cell Biol* 47, 41–51.
- Wilson C, Venditti R, Rega LR, Colanzi A, D'Angelo G, De Matteis MA (2011). The Golgi apparatus: an organelle with multiple complex functions. *Biochem J* 433, 1–9.
- Wong KA, Wilson J, Russo A, Wang L, Okur MN, Wang X, Martin NP, Scappini E, Carnegie GK, O'Bryan JP (2012). Intersectin (ITSN) family of scaffolds function as molecular hubs in protein interaction networks. *PLoS One* 7, e36023.
- Wu SK, Gomez GA, Michael M, Verma S, Cox HL, Lefevre JG, Parton RG, Hamilton NA, Neufeld Z, Yap AS (2014). Cortical F-actin stabilization generates apical-lateral patterns of junctional contractility that integrate cells into epithelia. *Nat Cell Biol* 16, 161–178.
- Yadav S, Puri S, Linstedt AD (2009). A primary role for Golgi positioning in directed secretion, cell polarity, and wound healing. *Mol Biol Cell* 20, 1721–1736.
- Yu Y, Chu PY, Bowser DN, Keating DJ, Dubach D, Harper I, Tkalcevic J, Finkelstein DI, Pritchard MA (2008). Mice deficient for the chromosome 21 ortholog *Its1n* exhibit vesicle-trafficking abnormalities. *Hum Mol Genet* 17, 3281–3290.
- Zegers MM, Zaal KJ, van IJendoorn SC, Klappe K, Hoekstra D (1998). Actin filaments and microtubules are involved in different membrane traffic pathways that transport sphingolipids to the apical surface of polarized HepG2 cells. *Mol Biol Cell* 9, 1931–1949.